

JGR Atmospheres

RESEARCH ARTICLE

10.1029/2022JD038048

Special Section:

Land-atmosphere coupling: measurement, modelling and analysis

Key Points:

- High-resolution land use/land cover (LULC), anthropogenic heat (AH), and urban canopy parameters (UCP) data sets are developed to examine the impacts of urban information on the urban thermal environment
- Relative contributions of LULC, AH, UCP, and AH + UCP on the 2-m temperature (T_2) are 54.82% (0.91°C), 11.45% (0.19°C), 7.83% (0.13°C), and 25.9% (0.43°C), respectively
- LULC and UCP impact T_2 by changing thermal and dynamical fields, while AH directly affects T_2 by enhancing sensible heat flux

Supporting Information:

Supporting Information may be found in the online version of this article.

Correspondence to:

S. Miao,
sgmiao@ium.cn

Citation:

Wang, J., Miao, S., Doan, Q.-V., Chen, F., Abolafia-Rosenzweig, R., Yang, L., et al. (2023). Quantifying the impacts of high-resolution urban information on the urban thermal environment. *Journal of Geophysical Research: Atmospheres*, 128, e2022JD038048. <https://doi.org/10.1029/2022JD038048>

Received 19 OCT 2022

Accepted 23 FEB 2023

Author Contributions:

Conceptualization: Jie Wang, Shiguang Miao
Formal analysis: Jie Wang, Quang-Van Doan, Fei Chen
Funding acquisition: Shiguang Miao, Yizhou Zhang
Investigation: Shiguang Miao
Methodology: Jie Wang, Fei Chen, Long Yang, Yizhou Zhang
Project Administration: Shiguang Miao

© 2023 American Geophysical Union.
All Rights Reserved.

Quantifying the Impacts of High-Resolution Urban Information on the Urban Thermal Environment

Jie Wang^{1,2,3} , Shiguang Miao^{1,2} , Quang-Van Doan⁴ , Fei Chen⁵ , Ronnie Abolafia-Rosenzweig⁵ , Long Yang³ , Guwei Zhang^{1,2} , Yizhou Zhang^{1,2} , Jingjing Dou^{1,2}, and Youpeng Xu³

¹Institute of Urban Meteorology, China Meteorological Administration, Beijing, China, ²China Meteorological Administration Urban Meteorology Key Laboratory, Beijing, China, ³School of Geography and Ocean Science, Nanjing University, Nanjing, China, ⁴Center for Computational Sciences, University of Tsukuba, Tsukuba, Japan, ⁵National Center for Atmospheric Research, Boulder, CO, USA

Abstract Detailed urban information, including land use/land cover (LULC), anthropogenic heat (AH) release, and urban canopy parameters (UCP), play critical roles in meteorological field simulations. It is particularly relevant for the Weather Research and Forecasting (WRF) model coupled with the single-layer urban canopy model (SLUCM). Thus, we develop high-resolution LULC, AH, and UCP data sets for Nanjing, a megacity in China, and conduct a series of numerical experiments with WRF/SLUCM to evaluate the impacts of urban parameters on the urban thermal environment. Model simulations with LULC scenarios have good agreement with the observed 2-m temperature (T_2) with a correlation coefficient of around 0.85, and present strong spatial homogeneity due to the more realistic representation of urban categories. The LULC change directly decreases the surface wind speed and increases (decreases) the sensible (latent) heat flux (Q_{SH} (Q_{LH}))) in urban areas during the daytime; meanwhile increases Q_{SH} and releases ground heat storage (Q_{GH}) during the nighttime, resulting in urban warming by 0.91°C in urban areas, compared with the control simulation (CTL) that does not take into account urban surfaces. In the LULC experiments combined with the UCP or AH, the UCP change enhances Q_{SH} and releases more Q_{GH} during nighttime, which increases T_2 by 0.13°C relative to LULC simulation. Also, the UCP effect reduces surface roughness and increases the width of the urban canopy, resulting in slightly enhanced wind speed, which is favorable for a warming environment in the urban area; the AH change contributes to increasing T_2 by 0.19°C through directly enhancing Q_{SH} relative to LULC simulation. AH combined with the UCP further strengthens the UCP effect in the urban area. Overall, the influence of urban parameters on the T_2 is more pronounced during nighttime than daytime, which presents a decreasing trend with an increase in wind speed and spatial humidity in the urban area.

Plain Language Summary Detailed information, describing urban land cover/land cover, anthropogenic heat release, and urban canopy parameters can considerably influence the urban thermal environment. However, the effect and the inter-comparison of these parameters have not been comprehensively investigated. In this study, we develop a high-resolution urban information data set for a megacity in China, Nanjing, and conduct a series of numerical experiments with WRF/SLUCM to evaluate the sensitivity of the urban thermal environment to the newly developed data set. We find that the urban thermal environment is most sensitive to urban land use, relative to nonurban scenarios. The relative contributions of urban land cover/land cover, anthropogenic heat release, urban canopy parameters, and anthropogenic heat release combined with urban canopy parameters on the average 2-m air temperature over the urban area are 54.82% (0.91°C), 11.45% (0.19°C), 7.83% (0.13°C), and 25.9% (0.43°C), respectively. These effects are more pronounced during nighttime than daytime, and present a decreasing trend with wind speed and spatial humidity increasing. This study provides insights on the impacts of urban information on the urban thermal environment and demonstrates the vital role of urban information in modeling urban temperature.

1. Introduction

More than half of the world's population currently lives in cities, and this proportion is projected to reach 70% by 2050 (Nations et al., 2019). Accompanied by the increasing population, land use/cover conversion from natural environments to urban environments eventually modifies the physical properties of the land surface (such as thermal inertia, roughness length, and anthropogenic heat released from human activities). These properties

Software: Jie Wang, Yizhou Zhang, Jingjing Dou
Supervision: Shiguang Miao
Visualization: Jie Wang, Quang-Van Doan
Writing – original draft: Jie Wang
Writing – review & editing: Quang-Van Doan, Long Yang, Guwei Zhang

modulate the energy, momentum, and mass exchanges between the land surface and atmosphere, and thus urbanization alters local urban climates (Chen, Miao, et al., 2011; Grossman-Clarke et al., 2010; Kim et al., 2021; Mohan & Kandy, 2015). The most representative climate phenomenon associated with urbanization is the urban heat island (UHI) effect, which is defined as significantly warmer temperatures in urban areas compared to their surrounding rural areas (Oke, 1982, 1987). Combined impacts of UHI with greenhouse-gas-induced global warming are predicted to cause increasing extreme heat conditions which have adverse impacts on the well-being of those living in urban areas (Argüeso et al., 2014; Doan et al., 2019; Georgescu et al., 2013; Vahmani et al., 2016; Yang et al., 2019; Zhang et al., 2021).

Studies on UHI have received a great deal of attention in recent years due to its importance on public health. UHI was first discovered in London in 1833 (Howard, 1833), and later-on became recognized in many cities worldwide (Bornstein, 1968; Hamdi et al., 2009; Miao et al., 2009; Salamanca & Mahalov, 2019; Streutker, 2010). Traditionally, UHI studies employed observational data to detect and describe the UHI effect; however, the numerical approach has recently become popular as an urban climate characterization. For instance, Bornstein (1968) revealed the UHI effect through an instrumented helicopter in New York City, and found that UHI was a maximum near the surface and decreased to zero at 300 m. Streutker (2010) studied the UHI effect in Houston with a remote sensing approach and found that the UHI was inversely correlated with rural temperature, but the spatial extent was found to be independent of both heat island magnitude and rural temperature. Salamanca and Mahalov (2019) examined the summer-time and winter-time variations of UHI for the Phoenix metropolitan area using remotely sensed and near-surface meteorological observations and reported that the higher surface UHI was found at night and during the warm season. Although these observational studies are invaluable in identifying the actual UHI effect, they have limited capacity in providing a mechanistic understanding of the underlying factors of UHI effect.

Numerical models can be a valuable tool in quantifying the urbanization impact on regional climate. Chen, Kusaka, et al. (2011) developed an integrated urban modeling system, including bulk urban parameterization (BULK) (Liu et al., 2006), the single-layer urban canopy model (SLUCM) (Kusaka & Kimura, 2004), the multi-layer building effect parameterization (BEP) (Martilli et al., 2002), and the simple building energy model (BEM) (Salamanca et al., 2010) coupled to BEP. The Weather Research and Forecasting (WRF), coupled with the integrated urban modeling system, has been widely used to address urban thermal environmental issues in various metropolitan areas. Each urban scheme has unique methods of parameterizing urban surfaces. In the original WRF/SLUCM model, the AH emission values are simply assigned and use a spatially uniform AH profile, when the land use category in the model grid cell is identified as “urban.” Moreover, the urban morphology parameters, such as UCP, are specified from a lookup table. Therefore, a considerable high-resolution WRF model simulation can provide near-surface intraurban variability but detailed urban information is required. These detailed model simulations can leverage urban structures data from the World Urban Database and Access Portal Tool (WUDAPT), which maps landscapes into 17 categories, including 10 classes of build-up areas and seven classes of natural areas (Ching et al., 2018; Stewart & Oke, 2012). Each urban category has associated variables associated with urban morphology and material properties, as described in Stewart and Oke (2012). Furthermore, developing the spatially heterogeneous AH data is critical for urban effect representation in climate models. For example, the AH database for China with a high spatial resolution of 500 m was developed by Hu (2020) with the construction AH estimation scheme, which can be used to simulate the urban environment and climate.

Several studies have discussed the necessity of realistically representing urban LULC, AH, and detailed building properties for improving urban thermal modeling (Chen et al., 2014; Doan et al., 2019; He et al., 2019; Kim et al., 2021; Li et al., 2018; Sun et al., 2021). He et al. (2019) applied the WRF with SLUCM to evaluate the impact of impervious surface area on the UHI in Berlin. The results showed that the simulated 2-m air temperature (T_2) matched the observations well, and fitted a well-linear function of simulated T_2 in the impervious surface area. Chen et al. (2014) updated urban land use data in the WRF coupled with SLUCM, showing better model performance of T_2 in Hangzhou. Doan et al. (2019) developed a two-dimensional AH data set with a top-down approach and used it to simulate the past, current, and future UHI effects in Hanoi, Vietnam. Kim et al. (2021) introduced AH and building height (ZH) into the WRF, demonstrating that AH and ZH can influence the representation of UHI and urban cool island (UCI). He et al. (2019) and Sun et al. (2021) developed urban canopy parameters (UCP) and applied them to the WRF to investigate the effects of UCP on the meteorological variables in Beijing and Nanjing city, respectively. Those studies, together with some other research (e.g., Chen, Miao, et al., 2011; Doan & Kusaka, 2016; Kusaka et al., 2012, 2016; Salamanca et al., 2011, 2018),

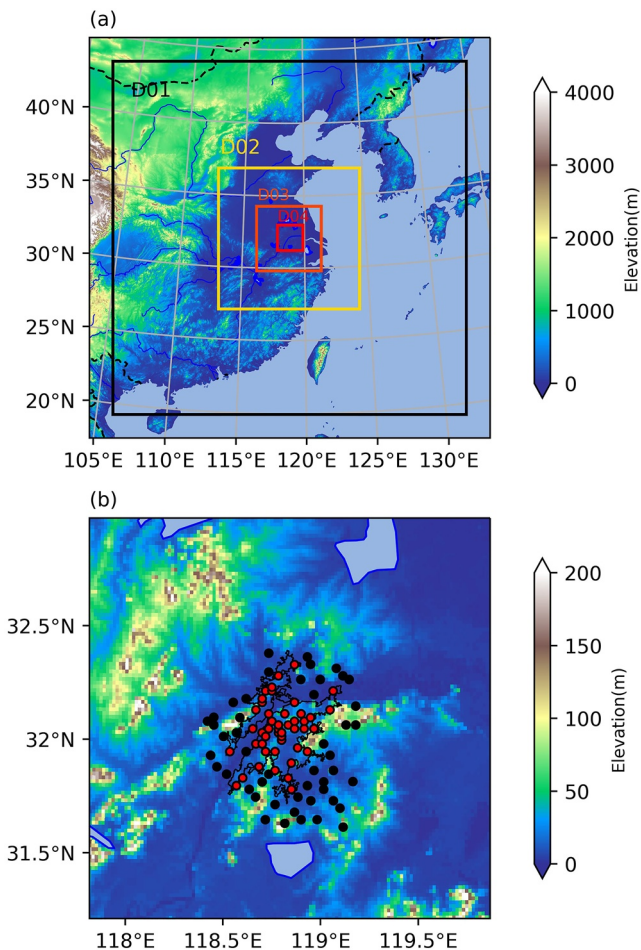


Figure 1. (a) Configuration of the four two-way nested domains for the Weather Research and Forecasting (WRF) simulations in Nanjing. (b) The inner domain D04. The black polygon shows the urban boundary of Nanjing; the shading represents the terrain (in m). Red and Black dots represent the urban and rural gauges that record surface air temperature from 00:00 UTC 10 May 2017 to 00:00 UTC 1 July 2017, respectively.

period are discarded for climatological analyses (see Section 3). The urban boundary of Nanjing, from the global urban boundaries data set (Li et al., 2020), is used to classify the urban or rural stations. If the station is located within the urban boundary it is already classified as an urban station; otherwise, it is a rural station. The 63 stations are divided into 34 urban stations and 29 rural stations based on the urban boundary of Nanjing. The urban stations mainly serve the purpose of model evaluation.

2.2. WRF Configuration

Simulations are implemented from 00:00 universal time coordinated (UTC) 1 May 2017 to 00:00 UTC 1 July 2017, to evaluate the impact of urban parameters on the urban thermal environment under different weather conditions. The first 10 days of simulations are considered model spin-up. A set of seven simulations are performed using the nonhydrostatic version of the WRF V4.3.1, coupled with the Noah land surface model. We set up four two-way nested domains (Figure 1) with the grid spacing (grid numbers) of 13.5 km (201×201), 4.5 km (241×241), 1.5 km (331×331), and 500 m (301×322). The coarsest domain (D01) comprises a major part of central and south-eastern China and the innermost domain (D04) centers over Nanjing (Figure 1b). We configured 39 vertical levels in the model. The upper boundary of the model is set at 50 hPa. We used the WRF single-moment six-class microphysics scheme, the Mellor-Yamada-Janjic boundary layer scheme, the Rapid Radiative Transfer Model for

highlight that the LULC, AH, and UCP play key roles in meteorological field simulations, and their accuracy is essential for improving the performance of the WRF model. However, these previous studies have primarily evaluated the sensitivity of single urban information in modeling the UHI using WRF coupled with an urban parameterization scheme. Fewer studies focus on developing entire urban parameters and assessing the critical differences in their sensitivities, especially for cities in China, where detailed AH and UCP data are rarely available. Furthermore, there are limited studies investigating the integrated influence of those urban parameters, and representing different impacts on the urban thermal environment.

Therefore, the aim of this study is to investigate the influence of detailed LULC and LULC combined with detailed AH or/and UCP information on the simulation of the urban thermal environment. We take Nanjing, the capital city of Jiangsu province in Eastern China, where no complex terrain is close to the city (Figure 1) as a study area. We first develop high-resolution LULC, AH, and UCP data sets which contain the detailed urban land use categories, spatial AH emission, and urban morphological parameters for Nanjing city. We further investigate the impacts of this newly developed urban information on the urban thermal environment based on the WRF coupled with SLUCM. Finally, thermal and dynamical fields are used to mechanistically understand the influence of urban parameters on the urban thermal environment.

This paper is organized as follows. The WRF configuration, experimental design, and LULC, AH, and UCP data set construction are introduced in Section 2; Section 3 evaluates the impact of high-resolution LULC, AH, and UCP on the urban thermal environment; Section 4 discusses the influences of LULC, AH, and UCP on the urban thermal environment. Finally, the summary and conclusions are provided in Section 5.

2. Methodology and Data

2.1. Observations

There are 89 meteorological stations that provide hourly surface air temperature at 2-m from 10 May to 1 July 2017 (the location of the gauges is shown in Figure 1b). The data set is obtained from the Jiangsu Meteorological Service. It is strictly quality-controlled for accuracy and consistency during the study period. Twenty-six gauges that do not have complete records during the study

Table 1
Overview of the Simulation Cases With Different LULC, AH, and UCP

Experiment name	LULC	Urban fraction	AH	UCP
CTL	24 (USGU removed Build-up)	/	No	Look-up table
LULC_One	24 (USGU updated Build-up)	Look-up table	No	Look-up table
LULC_Three	33 (USGU + LIR + HIR + CIT)	Updated	No	Look-up table
LULC_WUDAPT	41 (USGU + LCZ1-10)	Updated	No	Look-up table
LULC_WUDAPT + AH	41 (USGU + LCZ1-10)	Updated	Updated	Look-up table
LULC_WUDAPT + UCP	41 (USGU + LCZ1-10)	Updated	No	Updated
LULC_WUDAPT + AH + UCP	41 (USGU + LCZ1-10)	Updated	Updated	Updated

Note. The “/” denoted the variable does not use in the simulation.

longwave radiation, Dudhia's scheme for short wave radiation, the Noah land surface model, and the Kain-Fritsch cumulus scheme (only turned on for the coarsest domain due to the fine spatial resolution of horizontal grids less than 10 km, e.g., Stensrud (2009)). All of which are extensively tested schemes for synoptic events in Nanjing (Yang et al., 2021). The WRF initial and boundary conditions are provided by the ERA5 reanalysis, with a 0.25° spatial resolution and 6-hr temporal resolution.

2.3. LULC, AH, and UCP Data and Numerical Experiment Design

Due to the potential discrepancy in UCMs (e.g., SLUCM, BEP, and BEP + BEM), we implement seven different sets of simulations with contrasting urbanization scenarios through coupling with SLUCM to the Noah land surface model. The aforementioned configurations are applied for each simulation scenario. Details of different simulation scenarios are summarized in the following section:

2.3.1. LULC Experiments

LULC change from natural surface to impervious surface changes in the physical properties of the land surface (e.g., thermal inertia, albedo, and roughness length), which influences dynamic characteristics and energy balance of the surface layer (Chen, Miao, et al., 2011; Doan et al., 2016; Kusaka et al., 2012; Miao et al., 2011; Salamanca et al., 2012). In the default WRF, the 24-category U.S. Geological Survey (USGS) global 1 km land cover map is used. However, the original USGS data set in WRF is obtained from 1992 to 1993, which does not represent the real urban land surface features due to the rapid land cover changes. Therefore, we construct three urban land cover maps in conjunction with USGS land cover and update them in the LULC experiments, such as LULC_One, LULC_Three, and LULC_WUDAPT, to investigate the effects of LULC on the urban thermal environment. For this group, the aforementioned model configurations are used for each set of the LULC simulation scenarios, and urban morphology parameters are specified from a lookup table (URBPARM.TBL). In the control simulation (CTL), the urban land use is replaced by the cropland land type (Figure 2a) to represent the zero-order effects of urban surfaces. Details for each simulation scenario are summarized below and in Table 1.

To represent the current urbanization condition of Nanjing, we obtained impervious surface data in 2017 from the 30 m FROM-GLC10 global landcover product (Gong et al., 2019). The accuracy of this product is higher 90%, and thus reasonably reflects the actual urban state (Gong et al., 2019). We resample these data to a 500 m resolution using the majority resampling principle and update the default urban land cover in the WRF innermost domain for the LULC_One simulation (Figure 2b). The urban fraction is fixed at 0.95 in the urban parameters table.

However, one urban land category combined with fixed urban fraction values cannot reproduce the intraurban variability correctly. In our study, we develop two other urban cover scenarios to examine the sensitivity of the urban thermal environment to urban categories in WRF. For the LULC_Three simulation, the urban grid cells are classified into three types based on the percentage of impervious converge (IR), low-intensity residential (LIR, $IR < 0.5$), high-intensity residential (HIR, $0.5 < IR < 0.8$), and commercial/industrial/transportation (CIT, $IR > 0.8$), as shown in Figure 2c (similarly with Yang et al., 2021), where the impervious surface extension agrees with that in LULC_One simulation. The default urban fraction for LULC_Three simulation is updated by a

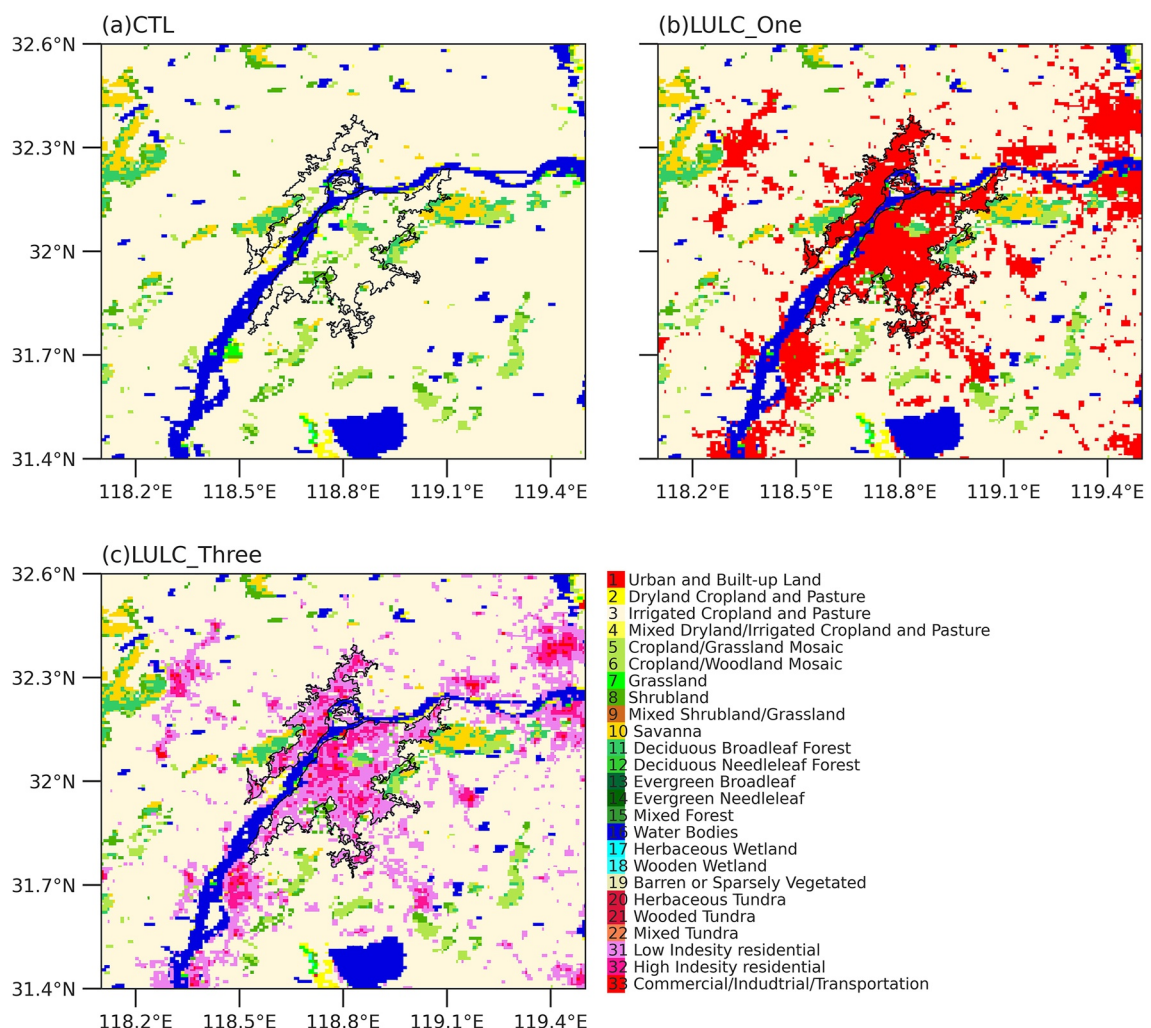


Figure 2. Land use categories for the D04 domain. (a) The control simulation (CTL) experiment, where the urban is replaced by the cropland; (b, c) are the land use/land cover (LULC) sensitivity experiments with one and three urban land use categories, respectively. The black polygon represents the urban boundary of Nanjing.

high-resolution (500 m) 2D spatial distribution of urban fraction (see Figure 6a), which is estimated according to the percentage of impervious convergence obtained from Gong et al. (2019). The urban morphology parameters are specified from the urban parameter lookup table.

For the LULC_WUDAPT simulation, urban areas are represented by the gridded Local Climate Zone (LCZ) map in Nanjing (Figure 3). The urban fraction is identical to the LULC_Three simulation. The LCZ map of Nanjing is created using the World Urban Database Access Portal Tool (WUDAPT) level 0, with 100 m resolution. It consists of the supervised classification of Landsat images using a Random Forest classification algorithm (Ching et al., 2018) using a three-part method. First, we obtain Landsat-8 satellite image with 30 m resolution in both the visible Near Infrared (NIR) and Shortwave Infrared (SWIR) Bands, and the Thermal Band (TIR) with 100 m resolution (Landsat ID of the scene is LC81200832017202LGN00). These data are imported to SAGA GIS to be projected and clipped to the region of interest (ROI). Second, we draw at least 20 homogeneous samples of training areas for the 10 urban landscape classes (LCZ 1–10) and the seven national landscape classes (LCZ A–G) using Google Earth (not shown). A detailed definition for LCZ classes can be found in Oke and Stewart (2012). Finally, we integrate the training sample and Landsat imagery into the SAGA platform and classify the LCZ with random forest algorithms. The classification accuracy for each iteration is evaluated via the ratio of the number of correctly classified pixels to the total pixels of the training sample in Figure 4. Based on the confusion matrix, the overall accuracy of LCZ classification maps is at least 85%, except for LCZ 1 (76.7%) which has the lowest sample density (Ren et al., 2019). The LCZ-based urban canopy parameters in the LULC_WUDAPT simulation

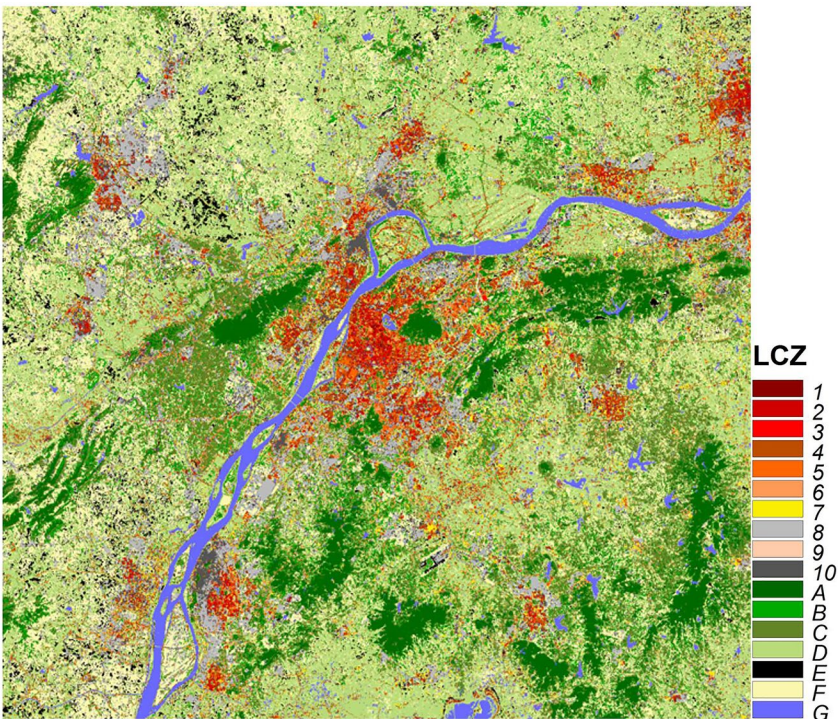


Figure 3. World Urban Database and Access Portal Tool (WUDAPT)-based Local Climate Zone (LCZ) map of Nanjing.

generally follow the data provided by Stewart and Oke (2012). The difference of simulated variables (e.g., T_2 , 10-m wind speed, and energy flux) between the LULC_WUDAPT simulation and CTL represents the impacts of the high-resolution WUDAPT urban land use on the simulated variables, hereon termed “LULC effect.”

Here, we provide a quantitative comparison between the percentage of urban land use and key geometrical features of urban canopy over Nanjing characterized by the three urban land use and WUDAPT categories. In the LULC_Three simulation, LIR and HIR are the most predominant land cover classes in the urban area (with the percentage of 69.26% and 28.69%, respectively), while CIT only accounts for 2.05% (Figure 5a). Corresponding to the LULC_Three simulation, we categorize the urban land use LCZ1-10 in the WUDAPT simulation into three groups, namely LCZ1-3, LCZ4-6, and LCZ7-10. It can be seen that the total proportion of LCZ4-6 (32.97%) and LCZ7-10 (49.52%) is larger than 80%; thus, they are the dominant land cover types in LULC_WUDAPT simulation (Figure 5b). In particular, 17.51% of the areas are covered by the LCZ1-3 in the LULC_WUDAPT simulation, which is larger than the CIT in the LULC_Three simulation (Figure 5b). Table 2 additionally presents several geometrical features of the urban canopy over Nanjing. The mean building height is 7.5 m in the LULC_Three simulation, while the mean value is 14.5 m in the LULC_WUDAPT simulation. The mean building and street widths are comparable between LULC_Three and LULC_WUDAPT simulation, suggesting that the higher and less dense urban buildings are characterized by WUDAPT than the three urban land use categories (Table 2).

2.3.2. AH Experiments

Anthropogenic heat (AH) emission is integrated into the urban canyon through the canopy model coupled with the WRF. As an important part, AH is considered in the energy balance equation ($Q^* + Q_F = Q_{SH} + Q_{LH} + Q_{GH}$, where Q^* is net all-wave radiation; Q_{SH} is sensible heat flux; Q_{LH} is latent heat flux; Q_{GH} is ground heat storage flux; Q_F is anthropogenic heat) (Oke, 1987). Despite AH being spatially heterogeneous in reality, in the default version of the SLUCM there is only one value of AH for each urban type. In this study, we evaluate the sensitivity of surface temperature to AH using a fine grid AH with 500×500 m (Figure 6b). The AH is estimated by the inventory method (Wang et al., 2020). The diurnal variation of AH is based on the default diurnal coefficient of the AH in the SLUCM. The gridded AH is considered in all urban grid points for the AH experiment to represent AH emissions in the urban area of Nanjing. As shown in Figure 6b, the AH intensity is particularly strong in the center of Nanjing where commercial complexes are located, and has a high population density.

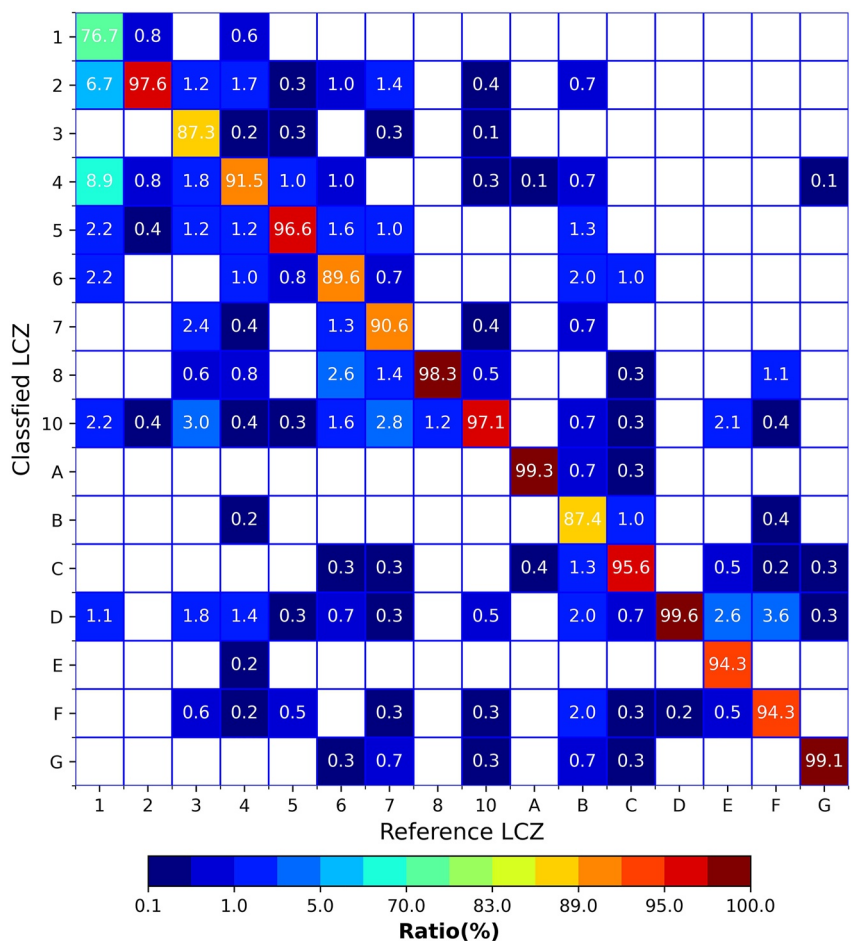


Figure 4. Accuracy matrix for the World Urban Database and Access Portal Tool (WUDAPT) Level 0 training areas, with training sample (reference Local Climate Zone (LCZ)) versus classified LCZ. The shading represents the ratio of a number of correctly classified pixels to the total pixels of the training sample for each class.

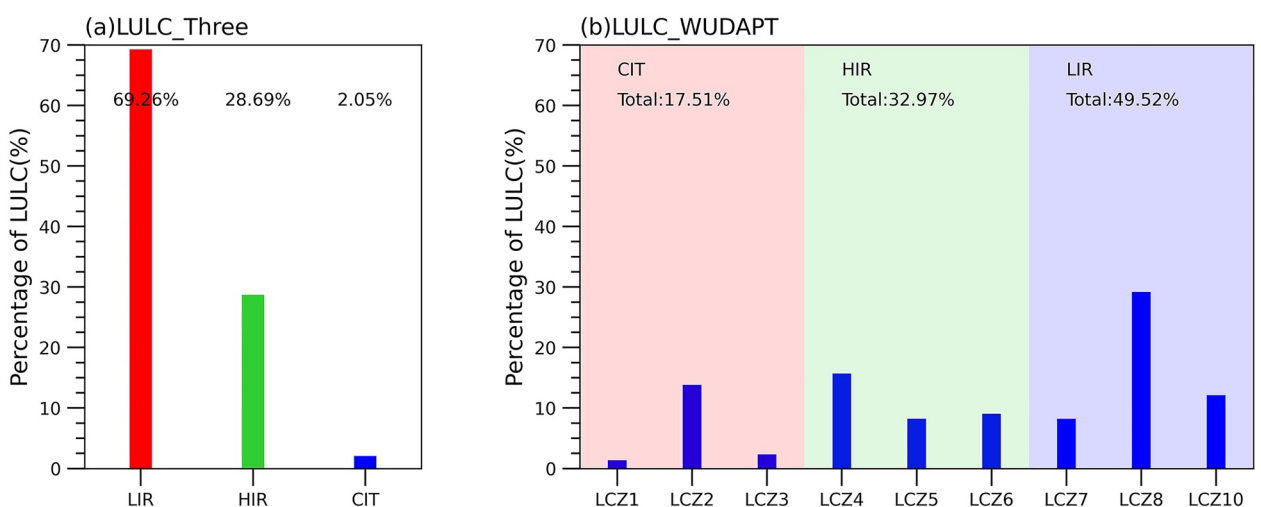


Figure 5. The percentage of each urban land use type to the total urban area in Nanjing city: (a) for LULC_Three simulation. low-intensity residential (LIR), high-intensity residential (HIR), and commercial/industrial/transportation (CIT) indicate the urban land use types. The values in the graph represent the proportion of each urban land use; (b) for LULC_WUDAPT simulation. LCZ1-10 shows the urban land use types. Corresponding to the LIR, HIR, CIT in (a), we categorize the urban land use LCZ1-10 into three groups, namely LCZ1-3, LCZ4-6, and LCZ7-10, which are denoted by different shading color in the graph.

Table 2
A List of Key Urban Morphology Parameters for Nanjing City in China

	Building height (m)	Building width (m)	Street width (m)
Three urban land use	7.5	9.23	9.23
WUDAPT	14.5	22.55	12.39
UCP	14.96	11.45	37.28

Differences between LULC_WUDAPT combined with AH simulation and LULC_WUDAPT simulation represent the impacts of AH, hereon termed “AH effect”.

2.3.3. UCP and AH Combined With UCP Experiments

Incorporating UCP in the SLUCM modifies the radiation balance equations, and thus impacts the temperature and heat fluxes over urban surfaces (wall, street, and roof; see more details in Masson (2000) and Kusaka et al. (2001)).

In the urban canyon, the urban morphology (e.g., building height (H), street width (SW), and building width (BW) determine the view factors between ground, wall, and sky, and consequently controls the radiation balance. The SW and BW can be calculated according to the building height (h_m), building surface ratio (λ_b), building plan area fraction (λ_p) as follows:

$$SW = \frac{2 \times h_m \times \lambda_p \times \left(\frac{f_{urb}}{\lambda_p} - 1 \right)}{(\lambda_b - \lambda_p)} \quad (1)$$

$$BW = \frac{2 \times h_m \times \lambda_p}{(\lambda_b - \lambda_p)} \quad (2)$$

where f_{urb} is urban fraction (as shown in Figure 6a); and h_m , λ_b , and λ_p are calculated as:

$$h_m = \frac{\sum_{i=1}^N A_i h_i}{\sum_{i=1}^N A_i} \quad (3)$$

$$\lambda_p = \frac{A_P}{A_T} \quad (4)$$

$$\lambda_b = \frac{A_R + A_W}{A_T} \quad (5)$$

where h_i is the height of building i ; N is the total number of buildings in the grid; A_i is the plan area on the ground level of the building i ; A_P is the plan area of buildings at ground level; A_T is the total plan area in a grid; A_R is the plan area of rooftops; and A_W is the total area of nonhorizontal roughness element surfaces, such as a wall.

The UCP used to calculate SW and BW is provided by the URBPARM.TBL and thus is a fixed value for each urban category (see detail in the URBPARM.TBL file). However, Sun et al. (2021) compared the default values

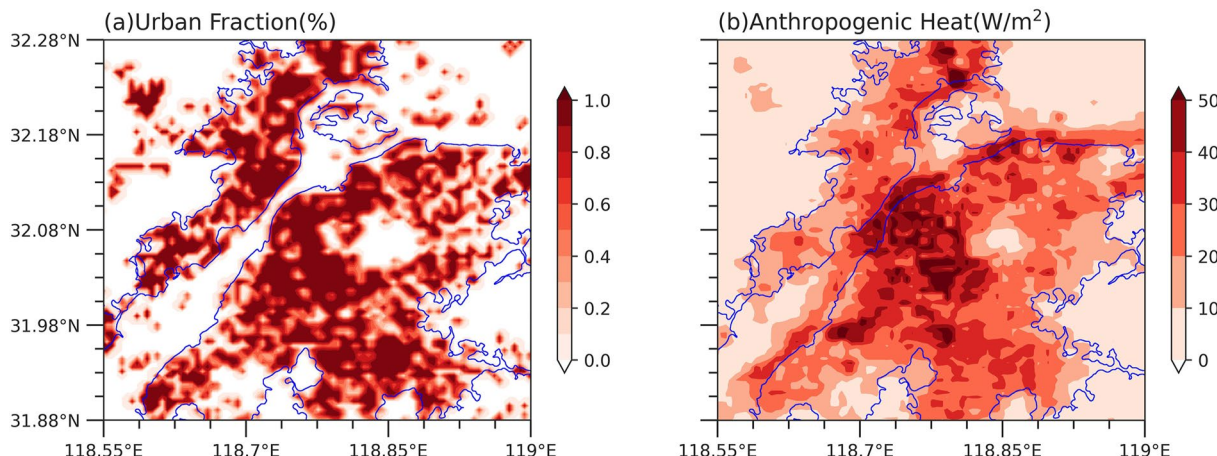


Figure 6. Spatial distribution of urban fraction (a) and anthropogenic heat (b) in Nanjing is used in numerical experiments. The urban fraction is calculated by the percentage of impervious converge within a 500 m grid. The anthropogenic heat (AH) map is obtained from Hu (2020). The blue polygon represents the urban boundary of Nanjing.

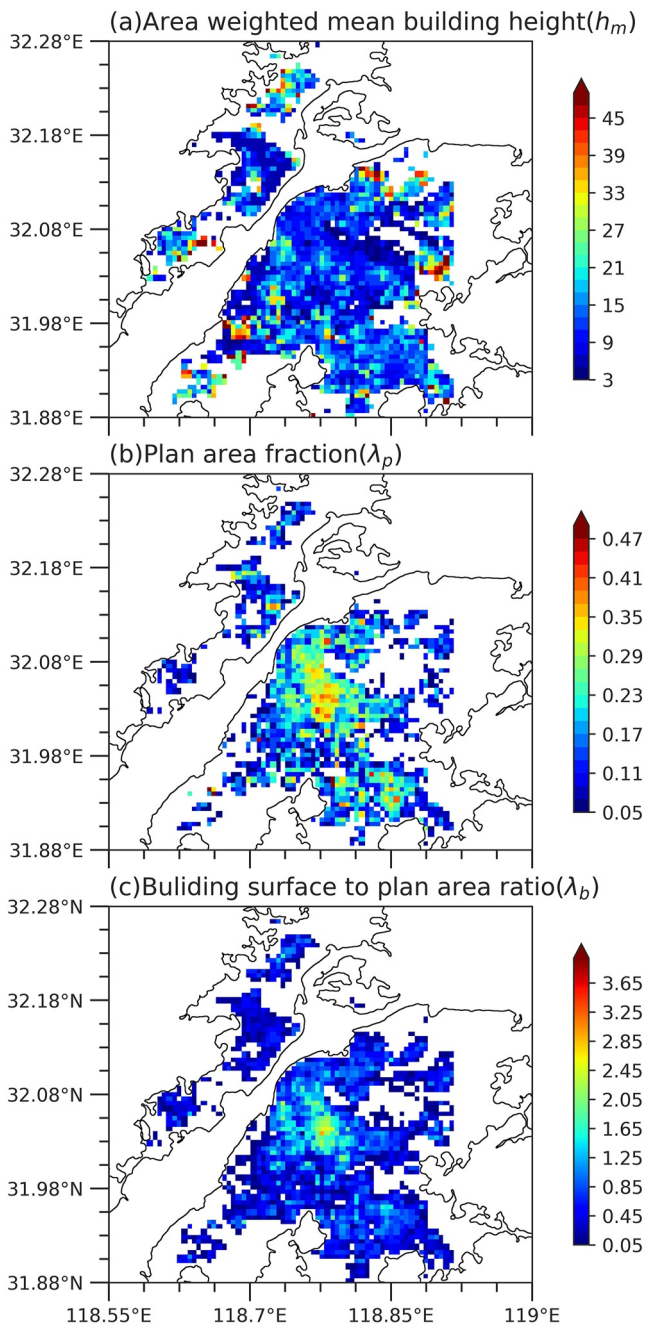


Figure 7. Spatial distribution of the gridded urban canopy parameters (UCP) for Nanjing: (a) area-weighted mean building height; (b) plan area fraction, and (c) building surface to plan area ratio. The black polygon is the urban boundary of Nanjing.

of UCP with actual local UCP in China's main cities, and found the WRF default values substantially underestimate the SW and slightly overestimate the BW. Thus, we estimate a high-resolution UCP data set for Nanjing with typical urban morphology parameters based on a vector-format archive of urban buildings for a collection of major cities in China (obtained from the website of Resource and Environment Science and Data Center of Institute of Geographic Sciences and Natural Resource Research in China). These data provide a series of attributes over the downtown area in Nanjing (Figure S1 in Supporting Information S1), for example, the floors (generally, the height of the residential building is 3 m), the building's footprint outline and perimeter, etc.

In this study, the vector-format archive of urban buildings in Nanjing is divided into 500 m grids to calculate the UCP. As shown in Figure 7, the maximum values of λ_p and λ_b are mainly located in the center of the city (Figures 7b and 7c), but the maximum values of h_m are distributed over the outer boundary of downtown Nanjing (Figure 7a). This is consistent with previous research showing low-rise buildings in the city center and buildings higher than 20 m being predominately located in the outer areas of Nanjing due to local land policy (Sun et al., 2021; Yang et al., 2021). This feature differs from the spatial pattern of building heights from the default look-up table which represents the highest buildings in the center of the city (CIT in Figure 2c and LCZ1-3 in Figure 3). Hence, the UCP gives more realistic urban canopy parameters. Therefore, we conduct simulations to investigate the influence of UCP on the urban thermal environment. In the LULC_WUDAPT + UCP simulations, AH is set to zero. Other parameters, except the urban canopy features over Nanjing that are characterized by the UCP, are the same setup as the LULC_WUDAPT simulations. The UCP effect is quantified as the difference between LULC_WUDAPT combined with UCP simulation and LULC_WUDAPT simulation, hereon termed “UCP effect.” In addition to the UCP simulations, the AH is integrated into the UCP simulations, where AH and UCP are used to examine the effect of AH and UCP on local meteorology. The difference between LULC_WUDAPT combined with AH and UCP simulation relative to the LULC_WUDAPT simulation represents the impacts of AH combined with UCP, hereon termed “AH + UCP effect.”

2.4. Model Evaluation Methods

Discrepancies between sensitivity simulations and observations are quantified by the evaluation metrics, including deviation (Bias), mean absolute error (MAE), root mean square error (RMSE), and correlation coefficient (CC). They are defined as the following:

$$\text{Bias} = \frac{1}{N} \sum_{i=1}^N (S_i - O_i) \quad (6)$$

$$\text{MAE} = \frac{1}{N} \sum_{i=1}^N |S_i - O_i| \quad (7)$$

$$\text{RMSE} = \sqrt{\frac{1}{N} \sum_{i=1}^N (S_i - O_i)^2} \quad (8)$$

$$CC = \frac{\sum_{i=1}^N (S_i - S')(O_i - O')}{\sqrt{\sum_{i=1}^N (S_i - S')^2} \sqrt{\sum_{i=1}^N (O_i - O')^2}} \quad (9)$$

where N is the number of hours in each time series, S_i is sensitivity simulation, and O_i is the observation at time-step i , and S' and O' are the average values from sensitivity simulations and observations, respectively.

3. Results

3.1. Evaluation of WRF-SLUCM Simulations

WRF simulated T_2 is evaluated at 34 urban observation stations within Nanjing (Figure 8). According to the spatial distribution of the observations, the urban center region is warmer than its surroundings during the analysis period, particularly for the commercial areas in the center of Nanjing (Figure 8a). Simulations match well with the observations, and capture the key features of T_2 spatial patterns in the urban area, except for the CTL simulation. Evaluation metrics comparing simulated and observed T_2 averaged across all 34 urban observation stations are shown in Table 3. The mean Bias, MAE, RMSE, and CC between simulated and observed T_2 are -0.23°C , 1.81°C , 2.21°C , and 0.84°C , respectively (Table 3). By comparison, the performances of LULC_Three and LULC_WUDAPT simulations are closer to the observation data with lower RMSE and higher CC values in Table 3. Thus, simulated T_2 captures the temporal variability of the observations in the urban area (Figure 9); however, the WRF model systematically underestimates the daily maximum temperature.

3.2. Impact of LULC on 2-m Temperature

The spatial distribution of T_2 simulated by the three urban land use scenarios are presented in Figures 8b–8d, and differences between them and the CTL simulation are plotted in Figure 10. The WRF model with one type of urban land use (LULC_One) leads to a warmer urban environment than CTL by 1.75°C in the urban area. Because of the fixed urban fraction values used in LULC_One simulation, the near-surface temperature does not accurately represent the spatial distribution differences in the urban area and extends to approximately the same area as the urban land use (see Figure 2b). By contrast, LULC_Three and LULC_WUDAPT simulations which incorporate the upgraded urban land cover, where land use conversion from single urban category to multicategorical urban land use, resulting in a lower hourly mean near-surface temperature with 0.91°C in LULC_Three and 1.01°C in LULC_WUDAPT simulation in the urban area of Nanjing (Figure 10). Compared with the LULC_One simulation, there is a significant spatial discrepancy of T_2 in multicategorical urban land use simulations. The variation of T_2 is very small in the center of the urban area, while it is significantly reduced in the urban areas with relatively low urban fraction values (in Figure 11d). In most parts of urban regions, the temperature declines up to 1.0°C . The reason is that the decrease in the urban fraction increases the proportion of green converging in each urban grid, resulting in an increase of surface evaporation, and then a decrease of T_2 , which is consistent with funding in previous studies (Li et al., 2019; Schatz & Kucharik, 2015). Additionally, a large hot spot of mean T_2 is modeled over the center of Nanjing by the LULC_Three and LULC_WUDAPT (Figures 10b and 10c). This is mostly consistent with the spatial distribution of observations in Figure 8a. These results suggested that considering the reasonable input land use and urban fraction could be an important factor in improving the T_2 simulation in urban areas (Salamanca et al., 2011, 2012).

Figures 11b and 11c show thermal responses at each urban classification in LULC_Three and LULC_WUDAPT simulations. For the LULC_Three simulation, the highest mean hourly T_2 occurs in CIT areas (increased by 1.06°C), followed by the HIR region (increased by 0.98°C), while the corresponding increase in the LIR area is the lowest (at 0.71°C). These simulations agree qualitatively with the observations that show the increased near-surface temperature in the CIT area is greater than that in the HIR and LIR areas. However, the mean hourly T_2 in Nanjing is not dominated by the CIT urban type because of its low areal coverage. Hence, HIR and LIR areas have a more pronounced effect on the T_2 , resulting in averaged T_2 increases by 0.91°C in the urban area.

The detailed impacts of LCZ 1–10 on the T_2 are shown in Figure 11c. The largest increases in T_2 are found in LCZ1-2 (compact high-rise and mid-rise), LCZ4-5 (open high-rise and midrise), and LCZ10 (heavy industry) with 1.30°C , 1.07°C , and 0.95°C increases, respectively. The lower T_2 in low-rise areas (e.g., LCZ3, LCZ6, and

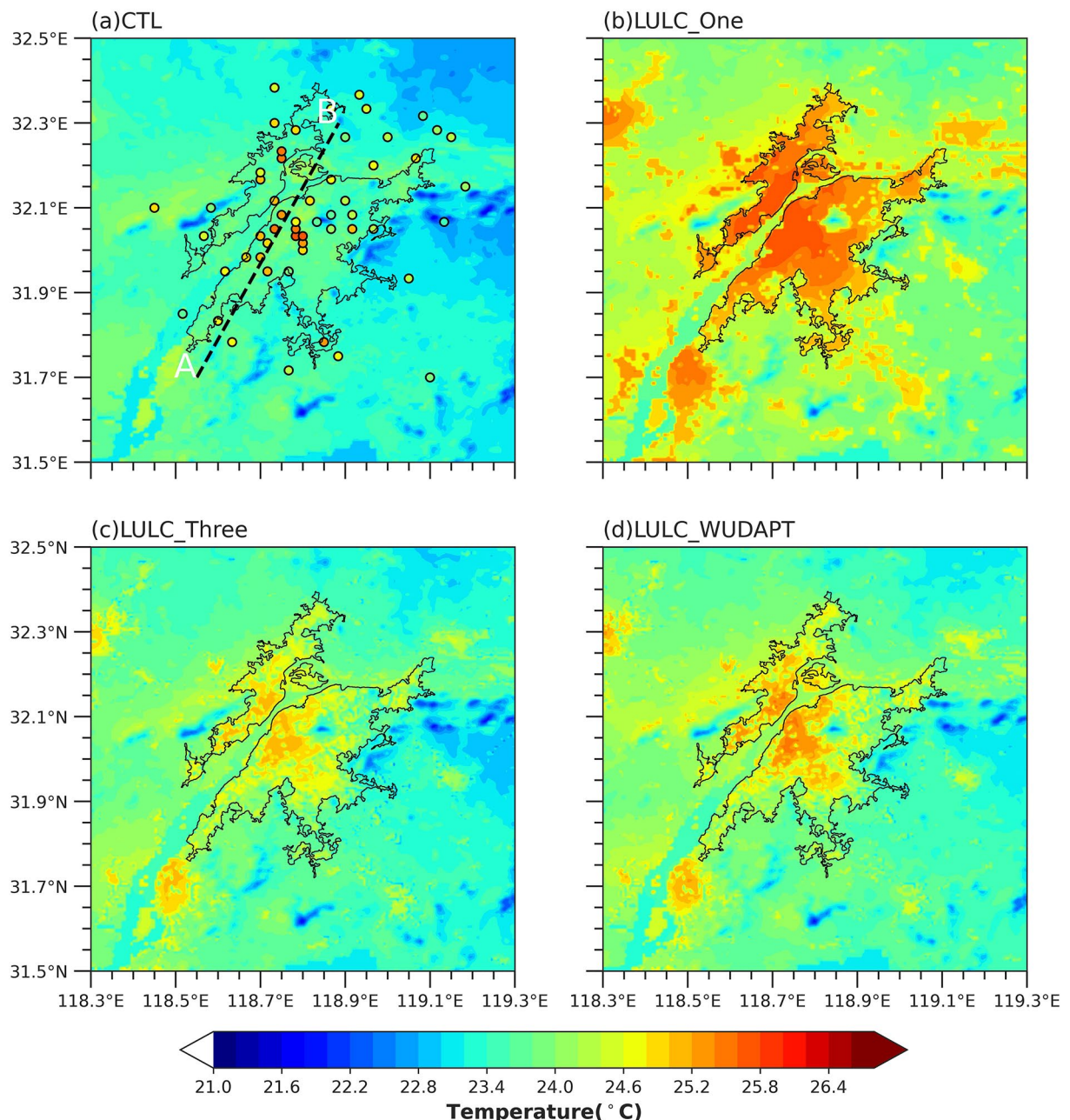


Figure 8. Spatial distribution of simulated mean hourly T_2 ($^{\circ}\text{C}$) from 00:00 UTC 10 May 2017 to 00:00 UTC 1 July 2017. Dots in (a) represent temperature observations from 63 meteorological stations. Blackline in (a–d) shows the urban boundary of Nanjing. The dashed line in (a) shows the position of the cross section (AB) for the vertical profile in Figure 17.

LCZ7) is expected. Thus, T_2 tends to reduce as building height and density decrease, which is similar to that shown in the LULC_One simulation. The multiple categories of urban land use result in relatively more spatial heterogeneous of T_2 in LULC_WUDAPT simulation relative to LULC_One simulation (Figure 11c); however, there are only minimal differences between the LULC_Three and LULC_WUDAPT simulations (Figures 10b and 10c). LCZ4-6 (32.97%) and LCZ7-10 (49.52%), which are the dominant land cover types (Figure 5b), control the near-surface temperature change in the urban area. Meanwhile, the increment of T_2 in LCZ4-6 and LCZ7-10 is close to that in HIR and LIR, resulting in similarities between T_2 in the LULC_WUDAPT simulation relative to the LULC_Three simulation. However, the LCZ1-3 in the LULC_WUDAPT simulation covers 17.51% of the urban areas, whereas the CIT in the LULC_Three simulation only covers 2.05%, and resulting in warmer T_2 in the

Table 3

Comparison of the Observed and Simulated 2-m Temperatures 00:00 UTC 10 May 2017 to 00:00 UTC 1 July 2017 at the 34 Gauges for the Model Performance

Experiment name	Bias (°C)	MAE	RMSE	CC
CTL	-1.24	2.03	2.46	0.87
LULC_One	0.29	1.81	2.34	0.83
LULC_Three	-0.59	1.85	2.03	0.85
LULC_WUDAPT	-0.40	1.78	2.25	0.85

center of the urban area from the LULC_WUDAPT simulation. In summary, LULC categories enhance the spatial heterogeneity of T_2 , resulting in more accurate near-surface temperatures at neighborhood scale from simulations that provide greater spatial detail of urban parameters.

3.3. Impact of AH, and UCP on the 2-m Temperature

The relative impacts of AH and UCP on T_2 are examined in Figures 11 and 12. The AH effect, that is, differences between LULC_WUDAPT simulation and LULC_WUDAPT + AH, which increases T_2 by 0.19°C is relatively weaker than the LULC effect (Figure 12a). The contribution of AH to T_2 in this study is comparable with those described by Chen et al. (2014) (29.7% (0.22°C)

in Hangzhou city of China) and (Yang et al., 2019) (below 1°C in the Yangtze River delta region). Note that the AH contributes to a linear increase in T_2 (Figure 11e), meaning that T_2 increases with increasing AH. This result highlights that AH is an important factor influencing the T_2 and the various values of AH can significantly change the spatial heterogeneity of T_2 in urban locations. By contrast, the UCP effect, that is, differences between LULC_WUDAPT and LULC_WUDAPT + UCP, is closely related to UCP distribution which increases the average T_2 by 0.13°C (Figure 12b). This phenomenon is presumably because the urban morphology parameters have been improved in the WRF model after employing UCP. Although the default mean building height in LULC_WUDAPT simulation (14.5 m based on the default look-up table) is lower than 14.96 m in the UCP, the building width is overestimated and the street width is underestimated in LULC_WUDAPT simulation (Table 2), which is consistent with the conclusion of Sun et al. (2021). Therefore, the wider urban canopy increases the shortwave radiation reaching the ground, which benefits the increase of T_2 (Boccalatte et al., 2020).

The combined effect of AH and UCP that is, the difference between LULC_WUDAPT simulation and LULC_WUDAPT + AH + UCP, is greater than the sum of its parts (i.e., the AH effect + the UCP effect) resulting in a 0.43°C warmer T_2 in urban areas (Figure 12c). Thus, the inclusion of gridded AH and UCP in Nanjing, compared with the values used by other previous studies (Wang et al., 2019; Yang et al., 2019, 2021), significantly affects urban surface temperature. We also examine how the T_2 is shifted due to UCP over each grid point as shown in Figures 11f and 11g. The main contribution of UCP to increased T_2 is in high-density urban areas with approximately 10 m of building height and 50 m of street width; while higher buildings with lower density are distributed mainly in the outer areas of Nanjing (Figure 6) where the UCP effect is relatively low. This is because the higher buildings and wider urban canopies result in a larger sky-view factor, and the shading effect of buildings on shortwave radiation is weakened during the daytime, resulting in increased T_2 (detail discussion in Section 4).

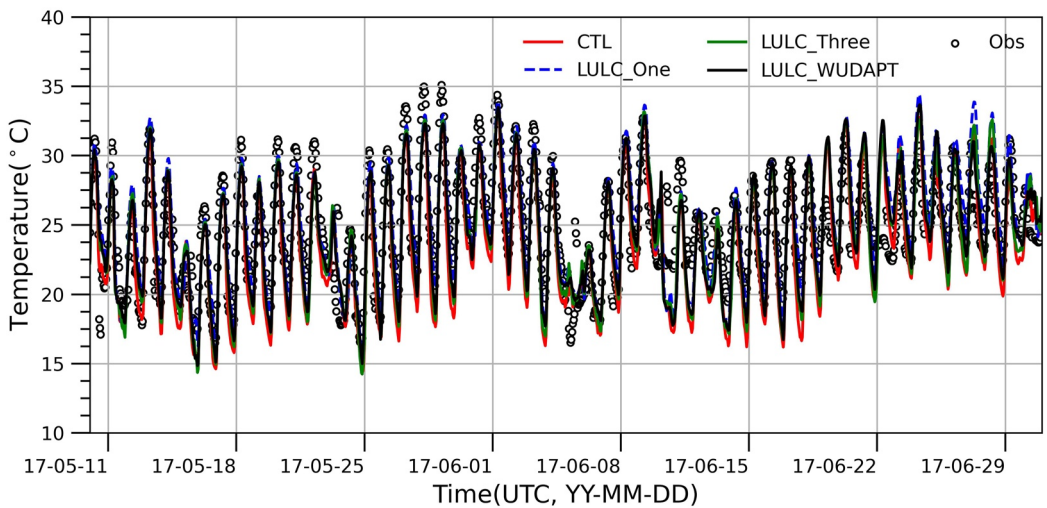


Figure 9. Time series of hourly 2-m temperature averaged over 34 gauges and the corresponding model grids in different simulations from 00:00 UTC 10 May 2017 to 00:00 UTC 1 July 2017, respectively. Dots show gauge-based observations.

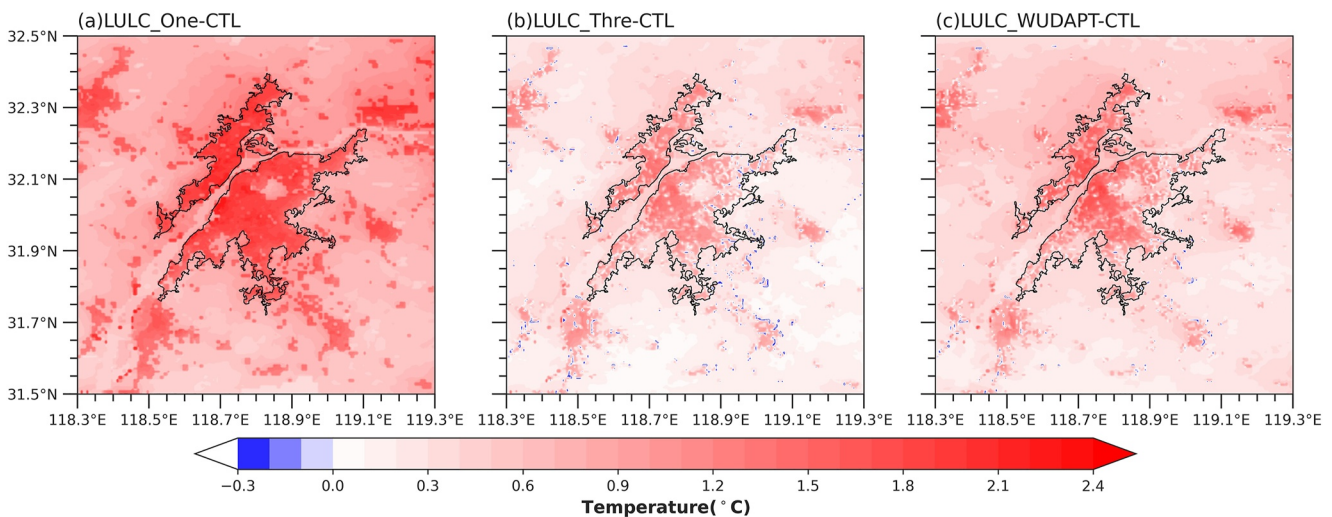


Figure 10. Differences in 2-m temperature averaged 00:00 UTC 10 May 2017 to 00:00 UTC 1 July 2017 between the (a) LULC_One, (b) LULC_Three, and (c) LULC_WUDAPT simulation and the control simulation (CTL). The black line shows the urban boundary of Nanjing.

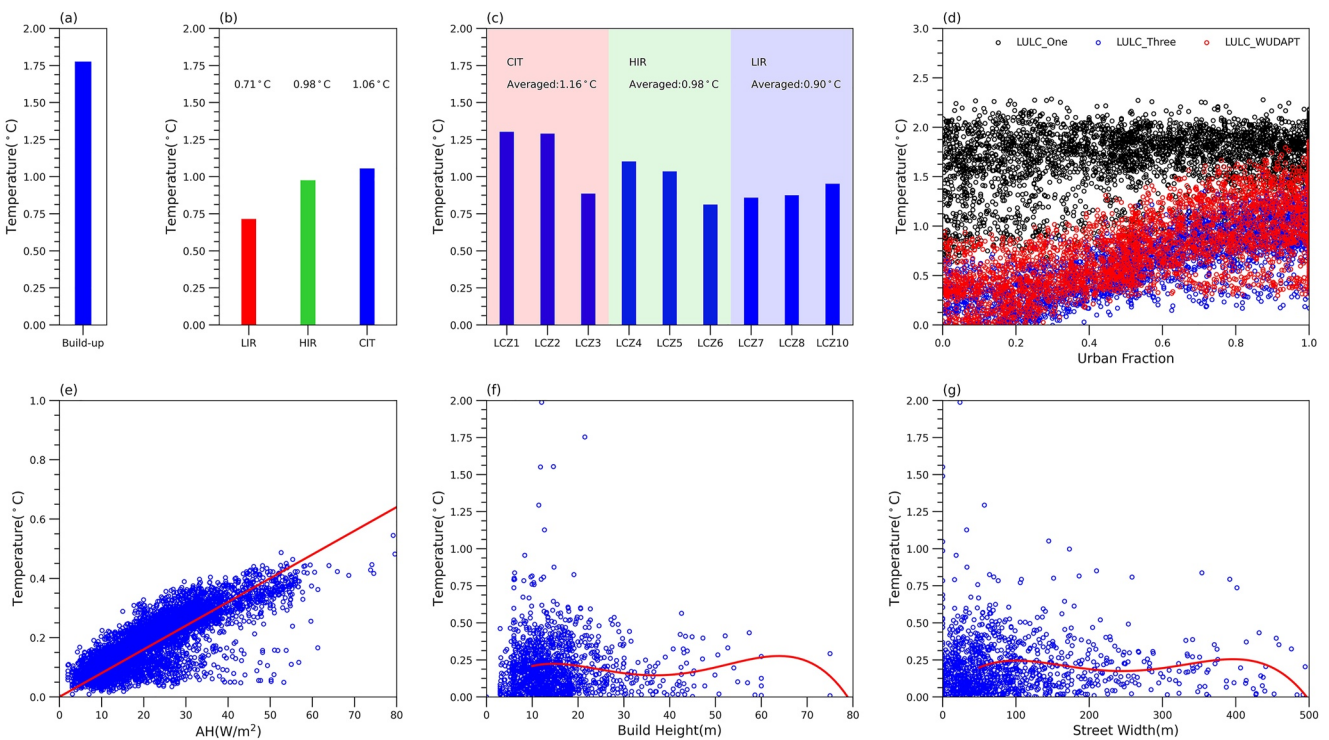


Figure 11. The histogram of the increment of averaged T_2 in urban area: (a) for LULC_One simulation with one urban category; (b) for LULC_Three simulation with three urban categories, including low-intensity residential (LIR), high-intensity residential (HIR), commercial/industrial/transportation (CIT); and (c) for LULC_WUDAPT simulation with 10 urban categories (e.g., LCZ1-LCZ10). Corresponding to the CIT, HIR, and LIR in panel (b), we categorize the urban land use LCZ1-10 into three groups and denote by different shading color in the graph. The Scatter diagrams of the relationship between the increment of simulated T_2 and the urban fraction (d), anthropogenic heat (AH) (e), building height (f), and street width (g) based on the results in Figures 10 and 12. Note that the urban fraction is fixed at 0.95 for the LULC_One simulation, while it is updated by a high-resolution (500 m) 2D data set for the LULC_Three and LULC_WUDAPT simulations (see Figure 6a). Panel (d) shows the pixel-to-pixel changes between the increment of averaged T_2 in LULC_One, LULC_Three, and LULC_WUDAPT simulations and 2D urban fraction data set.

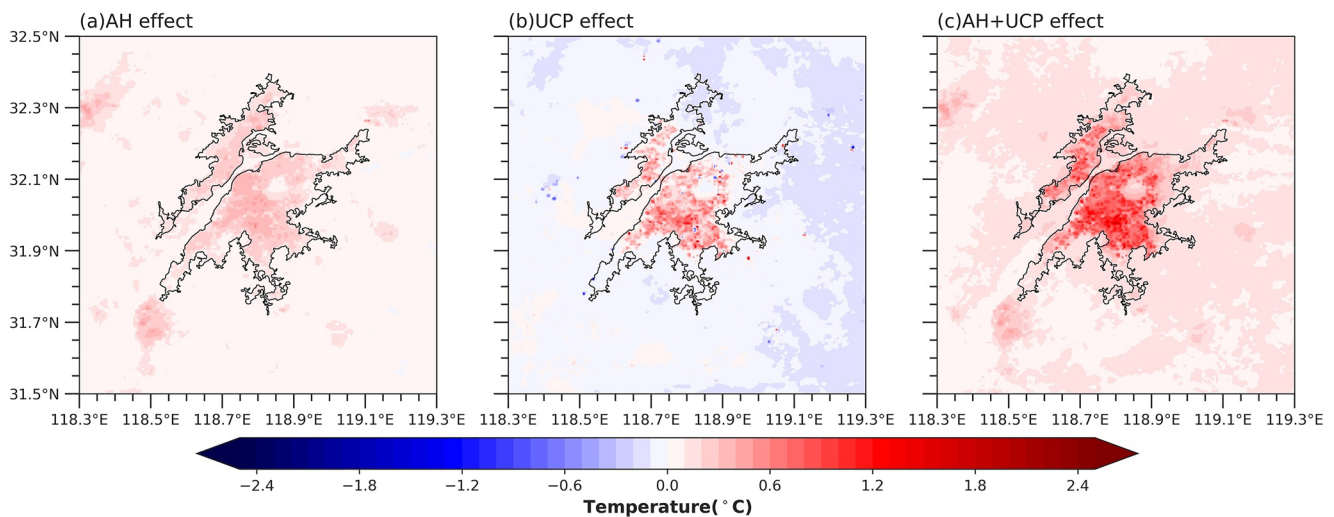


Figure 12. Spatial distribution of the increment of 2-m temperature averaged during 00:00 UTC 10 May 2017 to 00:00 UTC 1 July 2017 induced by: (a) anthropogenic heat (AH) effect; (b) urban canopy parameters (UCP) effect; (c) combined AH and UCP (AH + UCP) effect. The black line shows the urban boundary of Nanjing.

3.4. Effect of LULC, AH, and UCP on Diurnal Variations of 2-m Temperature

Figure 13 and Table 4 present the impacts of LULC, AH, and UCP on diurnal variations of T_2 . Compared with the CTL simulation (Figure 8a), LULC_WUDAPT simulates a remarkable warming effect with 0.06°C during the

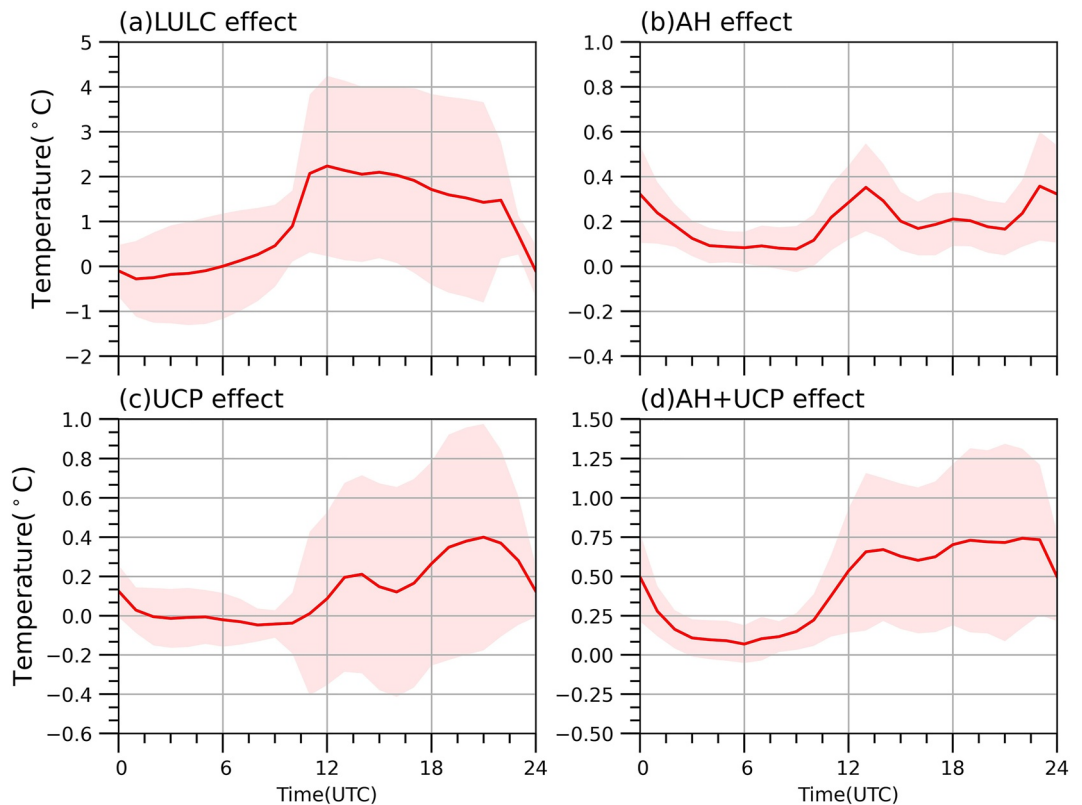


Figure 13. Diurnal variations of the increment of 2-m temperature induced by (a) land use and land cover (LULC) effect, anthropogenic heat (AH) effect, urban canopy parameters (UCP) effect, and combined AH and UCP (AH + UCP) effect averaged the urban pixels that correspond with the location of 43 urban gauges in different simulations over Nanjing. The red line denotes the averaged 2-m temperature.

Table 4

The Statistical Average Value of 2-m Temperature Induced by the LULC Effect, AH Effect, UCP Effect, and AH Combined With UCP Effect in the Urban Area During Daytime and Nighttime; Nighttime Is 11:00–21:00 UTC; Daytime Is 23:00–10:00 UTC

Effect	Daytime (°C)	Nighttime (°C)
LULC effect	0.06	1.77
AH effect	0.14	0.24
UCP effect	-0.01	0.23
AH + UCP effect	0.17	0.65

daytime and 1.77°C during the nighttime (Table 4). The UCP effect also shows noticeable nighttime warming (0.23°C) with minimal changes to daytime T_2 (-0.01°C) (Table 4). The AH effect results in warming throughout the day, with peaks at 14:00 and 23:00 UTC. This result is slightly different from the default diurnal cycle of the AH in the SLUCM which exhibits two peaks at 00:00 and 09:00 UTC, suggesting that urban warming lags the AH emission. When combined with UCP and AH effects, the diurnal variations of the T_2 is consistent with the UCP effect, with 0.65°C at night (Table 4), indicating that the diurnal profile of T_2 is mainly determined by the UCP effect due to the strong contribution of UCP to T_2 . Overall, the relative contributions of LULC, UCP, and AH combined with UCP effects to the T_2 averaged over the urban area are more pronounced during nighttime than during daytime. This result agrees with the theory of UHI formation in Oke (1982), as well as with the results from previous modeling studies (Giannaros et al., 2013; Li et al., 2014).

3.5. Differences Between LULC, AH, and UCP Effects Under Varying Synoptic Conditions

Results in Sections 3.1–3.4 show the impact of LULC, AH, and UCP effects on the increment of urban surface temperature, here, we further examine the influence of LULC, AH, and UCP effects under various synoptic

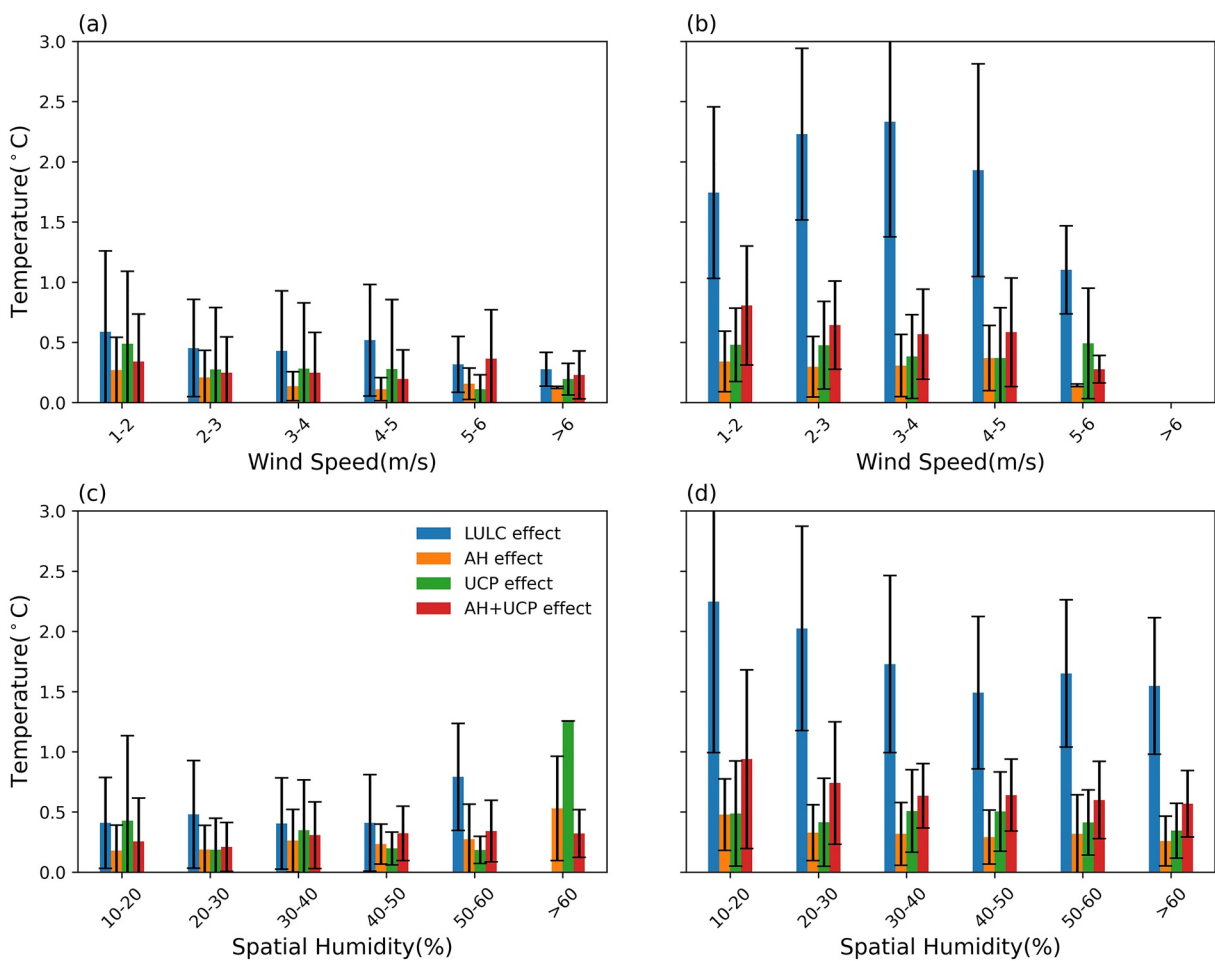


Figure 14. Changes of the increment of 2-m temperature over different ranges of (a, b) wind speed and (c, d) spatial humidity during daytime (left) and nighttime (right). Bars with different colors in each panel indicate the land use/land cover (LULC) effect, AH effect, urban canopy parameters (UCP) effect, and AH combined with the UCP effect.

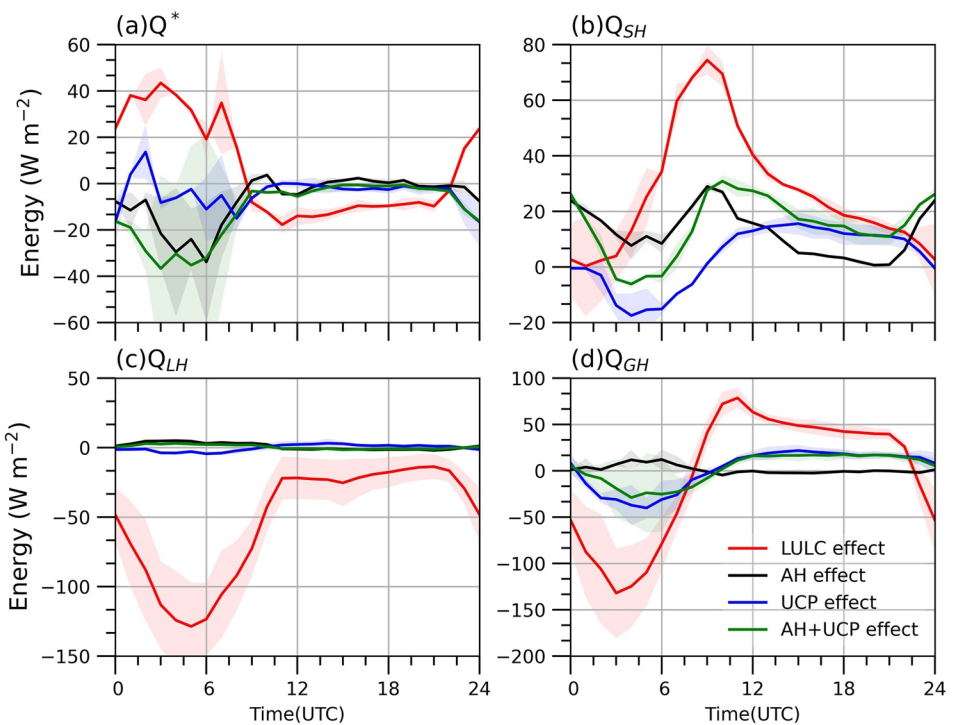


Figure 15. Simulated diurnal variations of the hourly mean surface energy flux due to land use/land cover (LULC), anthropogenic heat (AH), urban canopy parameters (UCP), and AH combined with UCP effect in the urban area from 00:00 UTC 10 May 2017 to 00:00 UTC 1 July 2017: (a) net all-wave radiation (Q^*); (b) sensible heat flux (Q_{SH}); (c) latent heat flux (Q_{LH}), and (d) ground heat storage (Q_{GH}).

conditions. T_2 declines with increases of 10-m wind speed, with this effect more pronounced during nighttime relative to daytime (Figure 14). It is noteworthy that the LULC effect on T_2 tends to increase with 10-m wind speed when wind speeds are lower than 4 m/s; conversely, the LULC effect on T_2 decreases with increasing wind speed for wind speed larger than 4 m/s. This result suggests that stable synoptic weather patterns associated with low wind speeds are conducive for enhancing urban heating; whereas strong wind speeds tend to carry heat away from the surface, resulting in reduced urban heating, especially at night. LULC, AH, UCP, and AH + UCP effect on nighttime T_2 decreases as the spatial humidity increases from 10% to 50%. Although T_2 is increased when spatial humidity is larger than 50%, the results are not representative due to the small sample size (Figure 14). These effects on T_2 reduce with increases in humidity because there is greater evaporative cooling in wetter conditions, and the relative humidity increases because of an increase in water vapor pressure and a decrease in saturation water vapor pressures when evaporation from the urban surface takes place (Kim & Baik, 2002). Overall, urban heating effects are more pronounced during nighttime than daytime across all evaluated synoptic conditions, excluding the UCP effect at very high humidity levels (>50%) since there are few data samples. Additionally, the LULC effect is dominant—relative to AH, UCP, and AH + UCP—across all evaluated synoptic conditions.

4. Discussion

4.1. Impact of LULC, AH, and UCP on the Surface Energy Budget

Differences between T_2 from the evaluated simulations (in Section 3) originates from discrepancies in how each simulation represents urban-related parameters and their corresponding effects on the surface energy budget. In this section, we discuss the impact of the LULC, AH, and UCP on the thermal environment due to the surface energy budget. Namely, net radiation (Q^*), sensible heat flux (Q_{SH}), latent heat flux (Q_{LH}), and ground heat storage (Q_{GH}), to investigate the influence mechanism.

Figure 15 presents impacts of LULC, AH, UCP, and AH combined with the UCP on the diurnal cycles of each surface energy flux in the urban area. In LULC simulation, where the natural surface is replaced by an urban

Table 5

The Statistical Average Value of Surface Energy Flux and 10-m Wind Speed for the LULC Effect, AH Effect, UCP Effect, and AH Combined With UCP Effect in the Urban Area During Daytime and Nighttime; Nighttime Is 11:00–21:00 UTC; Daytime Is 23:00–10:00 UTC

Variables		Daytime	Nighttime
Net all-wave radiation	LULC effect	27.32	-6.87
	AH effect	-15.96	-0.82
	UCP effect	-5.31	-3.21
	AH + UCP effect	-23.70	-3.78
Sensible heat flux	LULC effect	28.42	25.85
	AH effect	16.57	10.09
	UCP effect	-8.04	11.09
	AH + UCP effect	7.77	19.65
Latent heat flux	LULC effect	-96.49	-23.57
	AH effect	3.61	-0.78
	UCP effect	-2.56	1.43
	AH + UCP effect	2.13	-0.60
Ground heat storage	LULC effect	-70.25	38.90
	AH effect	5.46	-1.33
	UCP effect	-21.23	16.20
	AH + UCP effect	-15.17	14.14
10-m wind speed	LULC effect	-1.05	-0.58
	AH effect	0.02	0.08
	UCP effect	0.33	0.36
	AH + UCP effect	0.29	0.37

impermeable surface, there is reduced water in the land surface favoring to decreased Q_{LH} by 96.49 W m^{-2} during daytime (Figure 15c and Table 5). The LULC effect produces a higher T_2 (Figure 10) and strong turbulent kinetic energy (TKE) in the urban area (Figure S3 in Supporting Information S1), resulting in a dramatic increase of Q_{SH} by 28.42 W m^{-2} during the daytime (Table 5). Also, LULC effect results in a net increase Q_{GH} (with the mean value of 70.25 W m^{-2}), and thus more thermal energy is transported from the surface to the soil (Figure 15d and Table 5). Meanwhile, the buildings cause smaller sky-view factors from the sky to the ground, which quantify the shading effect inside the urban canyon, resulting in the decrease of Q_{GH} a few hours after sunrise; while Q_{GH} increases in the late afternoon since the shading depends on the solar angle. These effects cause an increase of Q^* during the daytime, providing positive feedback to T_2 in the urban area. By contrast, Figure 15 indicates the LULC effect mainly shows a positive Q_{SH} and Q_{GH} at night. The positive Q_{SH} continues into the night in the urban area, which remains the main determinant of air temperature. On the other hand, heat is transported from the soil to the surface at night. More heat storage in the walls and floor and release at night (Figure S2 in Supporting Information S1), which is especially favorable for maintaining a warmer environment during nighttime (Giannaros et al., 2018).

The influences of AH or/and UCP on the urban thermal environment are also discussed in this section. The influence of urban land use combined with AH and UCP on the Q^* and Q_{LH} is small; whereas its influence is obviously on the Q_{SH} and Q_{GH} . Since AH is directly added to the Q_{SH} in the SLUCM, so that the impact of AH on Q_{SH} is mostly consistent with AH (approximately 13.33 W m^{-2} , Figure 15b and Table 5). AH effect enhancement to Q_{SH} in turn enhances potential temperature during the daytime. However, the UCP effect shows significant differences with respect to surface energy flux, which finally results in a negative Q_{SH} . This is related to the weak TKE reducing atmospheric transport and mixing in the urban area during the daytime (Figure S3 in Supporting Information S1). Also, the UCP effect

makes a negative Q_{GH} , indicating more heat storage in the soil during the daytime. In the nighttime, UCP induces positive Q_{GH} values, meanings that increase building height and wider urban canopy in the urban area cause more heat transporting from the ground to the urban canopy, contributing to urban overwarming at night (Figure S2 in Supporting Information S1), which is similar to WRF simulation results of other cities in Seoul (Kim et al., 2021) and Guangzhou (Shen et al., 2019).

4.2. Impact of LULC, AH, and UCP on Dynamic Fields

The influences of LULC, AH, and UCP effect on the wind speed from 00:00 UTC 10 May 2017 to 00:00 UTC 01 July 2017 are analyzed in Figures 16 and 17. It is clear that the LULC effect causes a decreased wind speed in day and night (by 1.05 m/s and 0.58 m/s, respectively; Table 5). It is because the LULC increases building heights, resulting in an increase of surface roughness (Figure S4a in Supporting Information S1), which exerts a strong drag effect on the wind speed, then lost momentum and reduces the wind speed, although LULC effect increases near-surface temperature gradient. As a result, the higher buildings more easily trap the heat and reduce the heat loss in the urban canopy, which results in a higher near-surface temperature in the urban area (Liu et al., 2017). By contrast, the UCP effect causes increase wind speed in day and night (by 0.33 m/s and 0.36 m/s, respectively; Table 5). Compared with the building height in the LULC effect and UCP effect, the averaged building height in UCP (e.g., LCZ1-2, and LCZ4-5) is less than that in LULC_WUDAPT (Figure S5 in Supporting Information S1) which causes a reduction of urban roughness lengths (ζ_{0m}) in the center of the urban area (Figure S4b in Supporting Information S1), so that the drag effect of buildings slightly reduced in the urban area (Shen et al., 2022). On the other hand, the wider urban canopy increases the sky-view factor, resulting in an increase of shortwave radiation reaching the ground, which in turn increases T_2 and in turn increases the wind speed (Oke, 1982). AH contributes to a direct increase in the sensible heat flux in the SLUCM, resulting in surface warming (Kim

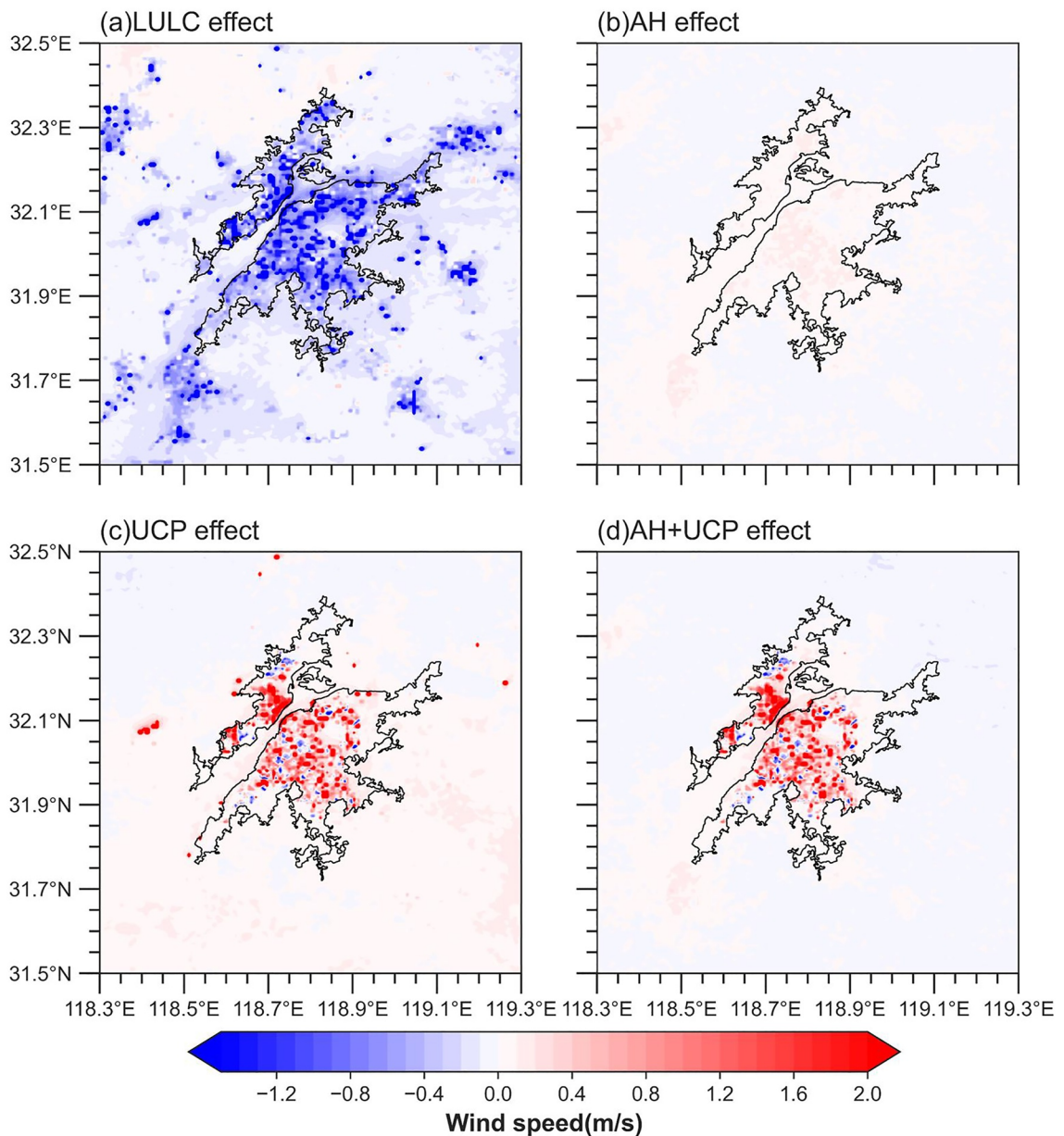


Figure 16. Impacts of land use/land cover (LULC), anthropogenic heat (AH), and urban canopy parameters (UCP) effect on averaged 10-m wind speed from 00:00 UTC 10 May 2017 to 00:00 UTC 1 July 2017. The black line shows the urban boundary of Nanjing.

et al., 2021), and in turn increases the surface wind speed due to the increasing near-surface temperature gradient (Souma et al., 2013). The AH combined with the UCP effect further led to an increase in wind speed with 0.37 m/s at night (Table 5). Overall, LULC, AH, and UCP effects on the wind speed are more pronounced during nighttime than daytime (not shown), which is consistent with their impacts on T_2 .

In addition to changes in near-surface wind speed, we also investigate how the LULC, AH, and UCP effect impacts propagate into the overlying atmosphere from 00:00 UTC 10 May 2017 to 00:00 UTC 1 July 2017 (Figure 17). The cross section along with A-B points in Figure 8a is selected to examine the influence of LULC, AH, and UCP effects on the atmospheric boundary layer structure over the urban area. The results show that the vertical wind speed in the urban canopy is more affected by the LULC effect. It can be seen that the LULC effect obviously reduces the wind speed with the most obvious impacts distributed in the center of the urban area. The LULC effect on wind speed reaches up to 900 hPa during the daytime, while remaining below 950 hPa at night.

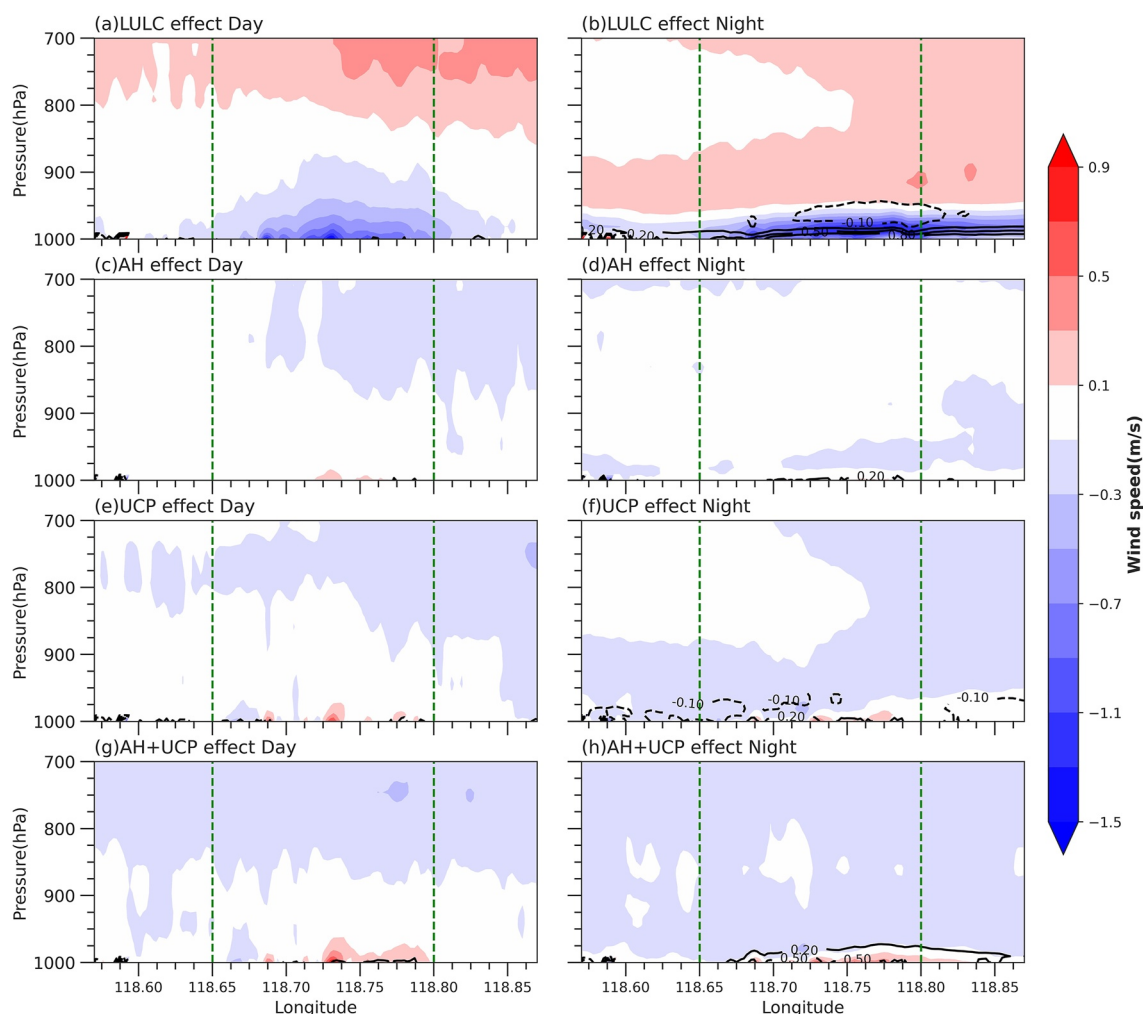


Figure 17. Vertical profiles of averaged vertical velocity (W-component of wind speed, shading, m/s) and potential temperature (black dashed contours, $^{\circ}\text{C}$) caused by the land use/land cover (LULC), anthropogenic heat (AH), and urban canopy parameters (UCP), and AH combined with the UCP effects along the cross section shown in Figure 8a on the daytime (23:00–10:00 UTC) and nighttime (11:00–21:00 UTC) from 00:00 UTC 10 May 2017 to 00:00 UTC 1 July 2017. The green vertical dashed lines along with the y axis show the urban extent.

This result suggests that the increased surface roughness caused by LULC effect has a considerable effect on the upper-air wind speed. In particular, the LULC effect increases the potential temperature but decreases the vertical wind speed at night (Figure 17b), we can infer that the dynamic-driven in terms of increased surface roughness in LULC effect on the wind speed reduction is more significant than the thermal impacts. In addition, AH led to surface warming, which increases the near-surface temperature gradient and then increases the surface wind speed. As shown in Figure 14, the slight increase in the atmospheric transport and mixing induced by weak wind speed in the urban area has the advantage of the storage of heat transfers between ground and air, especially at night, resulting in increases in near-surface temperature. Therefore, those results could explain the causes of the dynamic influence of LULC, AH, and UCP effects on the surface temperature by change surface wind speed.

5. Summary and Conclusions

This study developed high-resolution LULC categories, AH, and UCP data sets for a megacity, Nanjing, China, and evaluated the sensitivity of a numerical atmospheric model to these data sets. We conduct a series of numerical sensitivity simulations using WRF coupled with SLUCM f from 00:00 UTC 10 May 2017 to 00:00 UTC 1 July 2017. The dynamic and thermodynamic influence mechanisms of urban parameters are diagnosed by examining thermal and dynamical changes caused by detailed urban information. The main findings are summarized below.

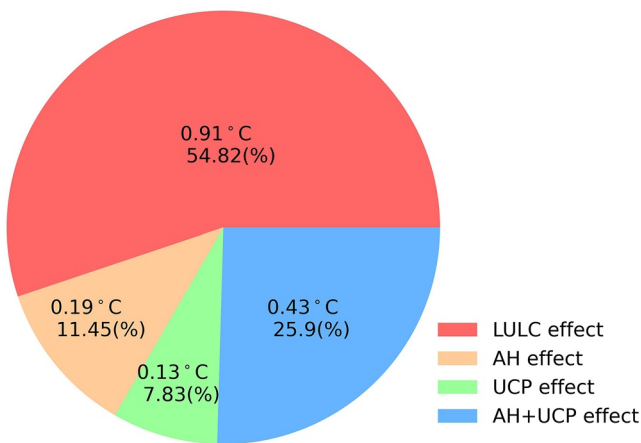


Figure 18. Pie charts showing the land use/land cover (LULC), anthropogenic heat (AH), and urban canopy parameters (UCP), and AH combined with UCP effect contributing to the 2-m temperature.

The simulated 2-m temperature (T_2) displays a good agreement with the observed temperature with a CC value of around 0.85, and shows a warmer center in the urban area. The spatial pattern of temperature has strong sensitivities to different urban representations in the WRF model. The spatial homogeneous of T_2 is accurately simulated by updating the urban land use, especially in the LULC_WUDAPT simulation due to the more realistic urban categories used.

The impacts of fine-scale LULC, AH, UCP, and AH combined with UCP on T_2 are investigated based on sensitivity simulations with different urban scenarios. Combined with LULC (here is WUDAPT urban land use), the natural underlying surface is replaced by the urban impermeable surface in the LULC simulation, which directly increases the sensible heat flux (Q_{SH}) and decreases the latent heat flux (Q_{LH}) in urban areas during the daytime. At night, the increased Q_{SH} and ground heat storage (Q_{GH}) is particularly favorable for maintaining a warmer environment during nighttime. Furthermore, the LULC effect decreases the surface wind speed by increasing surface roughness, which reduces the heat loss in the urban canopy, resulting in the mean T_2 increased by 0.91°C in urban areas (Figure 18).

AH directly increases the Q_{SH} in the SLUCM, resulting in a warmer mean T_2 by 0.19°C through increasing the Q_{SH} , rather than influencing the dynamic field (e.g., wind speed). The diurnal variation induced by the AH is not distinctly different between day and night periods; meanwhile, urban warming caused by the AH effect lags the associated enhanced Q_{SH} by 1–2 hr.

The UCP effect presents a negative Q_{SH} and Q_{GH} during the daytime, but increased the Q_{SH} and Q_{GH} during nighttime. This leads to the substantial heat flux transported from the ground to the urban canopy increasing the T_2 at night. The UCP effect slightly increases the wind speed; it seemed that the slight increase in the atmospheric transport and mixing in the urban area has the advantage of the storage of heat transfers from the ground to the air at night. The AH combined with the UCP effect further strengthens the UCP effect in the urban area. Overall, the relative contributions of LULC, AH, UCP, and AH combined with UCP on the T_2 averaged over the urban area are 54.82% (0.91°C), 11.45% (0.19°C), 7.83% (0.13°C), and 25.9% (0.43°C), respectively (Figure 18), which is more pronounced during nighttime than during daytime; and decreased with wind and spatial humidity increase.

The primary contribution of this study to previous literature is the comprehensive assessment of urban parameters, including LULC, AH, and UCP, on simulations of the urban thermal environment. Most previous studies discussed the impacts of single or limited variations of urban parameters, thus leaving insufficient insight into inter-parameter comparison (Chen et al., 2014; Kim et al., 2021; Li et al., 2019; Streutker, 2010). In this study, we contribute to understanding the differences between urban parameter components and explain the underlying physical and thermophysical processes. This knowledge is critical for urban climate modelers because more and more high-resolution modeling is required thanks to the advancement of computational ability and the higher need for fine-scale information for urban policymakers. In addition, the establishment and rapidly emerging urban informatics field allow more and more detailed observed urban information, from both in-situ measurement/observation and remote sensing techniques. Such abundantly available data allow more detailed urban information could be involved in urban climate modeling to inform high-resolution modeling.

However, we should admit that there are some limitations of this study related to the WRF/SLUCM model, although similar configurations are applied by a few other studies (e.g., Kim et al., 2021). For instance, the building height in the UCP is restricted to less than 75 m, hence the impact of tall buildings (larger than 75 m) cannot be implemented, such as the shading effect of tall buildings causes lower daytime temperature, the tall building in commercial/industrial areas increases the AH emission. Also, the AH, which is estimated by collecting energy consumption data and socioeconomic statistics and combined with multisource remotely sensed data (Wang et al., 2020), cannot reflect the daily variation of anthropogenic heat emission in the real world. Besides, the main purpose of our study is to evaluate the impact of urban factors and elucidate its influence mechanisms, thus the SLUCM is used rather than the multilayer UCM (i.e., BEP and BEP + BEM) because constructing an ideal urban environment would be more effective in identifying the urbanization effect (Kim et al., 2021).

In future research, we will establish localized anthropogenic heat emissions and study the effect of local nonuniform high-resolution anthropogenic heat emissions on thermal fields in the WRF coupled with multilayer UCM. Meanwhile, other urban parameters, such as building height, green roof fraction, street width, and so on, could impact the urban surface temperature. Thus, the influence of high-resolution urban factors similar to the real world on the urban climate should be further investigated. It helps us further estimate the magnitudes of local effects induced by urbanization.

Data Availability Statement

The updated land use/land cover data over the Nanjing region are available at an online repository http://data.ess.tsinghua.edu.cn/fromglc10_2017v01.html; the AH data are found online at <http://www.tpdc.ac.cn/zh-hans/data/637e99a1-be38-4a9f-8af9-a8600e13d568/>; the urban morphology parameters are obtained from <http://www.resdc.cn/data.aspx?DATAID=270>; the source code of WRF model Version 4.3.1 used in this study can be downloaded from https://www2.mmm.ucar.edu/wrf/users/download/get_sources.html.

Acknowledgments

This study is financially supported by the Natural Science Foundation of China (42205193), the Youth Beijing Scholars Program (Grant 2018-007), the Natural Science Foundation of China (41705088), and the Water System at the National Center for Atmospheric Research (NCAR), the NASA IDS Grant 80NSSC20K1262. The numerical simulations of the present work were calculated on the computing facilities in the High-Performance Computing Center (HPCC) of Nanjing University. We much appreciated the careful review and editing from Dr. Ronnie Abolafia-Rosenzweig at NCAR.

References

- Argüeso, D., Evans, J. P., Fita, L., & Bormann, K. J. (2014). Temperature response to future urbanization and climate change. *Climate Dynamics*, 42(7), 2183–2199. <https://doi.org/10.1007/s00382-013-1789-6>
- Boccalatte, A., Fossa, M., Gaillard, L., & Menezo, C. (2020). Microclimate and urban morphology effects on building energy demand in different European cities. *Energy and Buildings*, 224, 110129. <https://doi.org/10.1016/j.enbuild.2020.110129>
- Bornstein, R. D. (1968). Observations of the urban heat island effect in New York City. *Journal of Applied Meteorology and Climatology*, 7(4), 575–582. [https://doi.org/10.1175/1520-0450\(1968\)007<0575:OOTUHI>2.0.CO;2](https://doi.org/10.1175/1520-0450(1968)007<0575:OOTUHI>2.0.CO;2)
- Chen, F., Kusaka, H., Bornstein, R., Ching, J., Miao, S., Grossman-Clarke, S., et al. (2011). The integrated WRF/urban modeling system: Development, evaluation, and applications to urban environmental problems. *International Journal of Climatology*, 31(2), 273–288. <https://doi.org/10.1002/joc.2158>
- Chen, F., Miao, S., Tewari, M., Bao, J. W., & Kusaka, H. (2011). A numerical study of interactions between surface forcing and sea breeze circulations and their effects on stagnation in the greater Houston area. *Journal of Geophysical Research*, 116, D12105. <https://doi.org/10.1029/2010JD015533>
- Chen, F., Yang, X., & Zhu, W. (2014). WRF simulations of urban heat island under hot-weather synoptic conditions: The case study of Hangzhou City, China. *Atmospheric Research*, 138, 364–377. <https://doi.org/10.1016/j.atmosres.2013.12.005>
- Ching, J., Mills, G., Bechtel, B., See, L., Feddema, J., Wang, X., et al. (2018). Wudapt: An urban weather, climate, and environmental modeling infrastructure for the Anthropocene. *Bulletin of the American Meteorological Society*, 99(9), 1907–1924. <https://doi.org/10.1175/bams-d-16-0236.1>
- Doan, Q.-V., & Kusaka, H. (2016). Numerical study on regional climate change due to the rapid urbanization of greater Ho Chi Minh City's metropolitan area over the past 20 years. *International Journal of Climatology*, 36(10), 3633–3650. <https://doi.org/10.1002/joc.4582>
- Doan, V. Q., Kusaka, H., & Nguyen, T. M. (2019). Roles of past, present, and future land use and anthropogenic heat release changes on urban heat island effects in Hanoi, Vietnam: Numerical experiments with a regional climate model. *Sustainable Cities and Society*, 47, 101479. <https://doi.org/10.1016/j.scs.2019.101479>
- Georgescu, M., Moustaqui, M., Mahalov, A., & Duddia, J. (2013). Summer-time climate impacts of projected megapolitan expansion in Arizona. *Nature Climate Change*, 3(1), 37–41. <https://doi.org/10.1038/NCLIMATE1656>
- Giannaros, C., Nenes, A., Giannaros, T. M., Kourtidis, K., & Melas, D. (2018). A comprehensive approach for the simulation of the Urban Heat Island effect with the WRF/SLUCM modeling system: The case of Athens (Greece). *Atmospheric Research*, 201, 86–101. <https://doi.org/10.1016/j.atmosres.2017.10.015>
- Giannaros, T. M., Melas, D., Daglis, I. A., Keramitsoglou, I., & Kourtidis, K. (2013). Numerical study of the urban heat island over Athens (Greece) with the WRF model. *Atmospheric Environment*, 73, 103–111. <https://doi.org/10.1016/j.atmosenv.2013.02.055>
- Gong, P., Li, X., & Zhang, W. (2019). 40-Year (1978–2017) human settlement changes in China reflected by impervious surfaces from satellite remote sensing [Dataset]. *Science Bulletin*, 64(11), 756–763. <https://doi.org/10.1016/j.scib.2019.04.024>
- Grossman-Clarke, S., Zehnder, J. A., Loridan, T., & Grimmond, C. S. B. (2010). Contribution of land use changes to near-surface air temperatures during recent summer extreme heat events in the Phoenix Metropolitan area. *Journal of Applied Meteorology and Climatology*, 49(8), 1649–1664. <https://doi.org/10.1175/2010jamc2362.1>
- Hamdi, R., Deckmyn, A., Termonia, P., Demarée, G. R., Baguis, P., Vanhuyse, S., & Wolff, E. (2009). Effects of historical urbanization in the Brussels capital region on surface air temperature time series: A model study. *Journal of Applied Meteorology and Climatology*, 48(10), 2181–2196. <https://doi.org/10.1175/2009JAMC2140.1>
- He, X., Li, Y., Wang, X., Chen, L., Yu, B., Zhang, Y., & Miao, S. (2019). High-resolution dataset of urban canopy parameters for Beijing and its application to the integrated WRF/Urban modelling system. *Journal of Cleaner Production*, 208, 373–383. <https://doi.org/10.1016/j.jclepro.2018.10.086>
- Howard, L. (1833). *The Climate of London: Deduced from meteorological observations made in the metropolis and various places around it. Harvey and Darton.*
- Hu, D. (2020). Time-series anthropogenic heat flux of China land surface [Dataset]. National Tibetan Plateau/Third Pole Environment Data Center. https://doi.org/10.11888/Socioeco_tpdc.270403
- Kim, G., Cha, D. H., Song, C. K., & Kim, H. (2021). Impacts of anthropogenic heat and building height on urban precipitation over the Seoul metropolitan area in regional climate modeling. *Journal of Geophysical Research: Atmospheres*, 126, e2021JD035348. <https://doi.org/10.1029/2021JD035348>
- Kim, Y. H., & Baik, J. J. (2002). Maximum urban heat island intensity in Seoul. *Journal of Applied Meteorology and Climatology*, 41(6), 651–659. [https://doi.org/10.1175/1520-0450\(2002\)041<0651:MUHIII>2.0.CO;2](https://doi.org/10.1175/1520-0450(2002)041<0651:MUHIII>2.0.CO;2)

- Kusaka, H., Chen, F., Tewari, M., Dudhia, J., Gill, D. O., Duda, M. G., et al. (2012). Numerical simulation of urban heat island effect by the WRF model with 4-km grid increment: An inter-comparison study between the urban canopy model and slab model. *Journal of the Meteorological Society of Japan*, 90, 33–45. <https://doi.org/10.2151/jmsj.2012-B03>
- Kusaka, H., & Kimura, F. (2004). Coupling a single-layer urban canopy model with a simple atmospheric model: Impact on urban heat island simulation for an idealized case. *Journal of the Meteorological Society of Japan*, 82(1), 67–80. <https://doi.org/10.2151/jmsj.82.67>
- Kusaka, H., Kondo, H., Kikegawa, Y., & Kimura, F. (2001). A simple single-layer urban canopy model for atmospheric models: Comparison with multi-layer and slab models. *Boundary-Layer Meteorology*, 101(3), 329–358. <https://doi.org/10.1023/A:1019207923078>
- Kusaka, H., Suzuki-Parker, A., Aoyagi, T., Adachi, S. A., & Yamagata, Y. (2016). Assessment of RCM and urban scenarios uncertainties in the climate projections for August in the 2050s in Tokyo. *Climatic Change*, 137(3–4), 427–438. <https://doi.org/10.1007/s10584-016-1693-2>
- Li, H., Zhou, Y., Wang, X., Zhou, X., Zhang, H., & Sodoudi, S. (2019). Quantifying Urban Heat Island intensity and its physical mechanism using WRF/UCM. *Science of the Total Environment*, 650(2), 3110–3119. <https://doi.org/10.1016/j.scitotenv.2018.10.025>
- Li, M., Song, Y., Huang, X., Li, J., Mao, Y., Zhu, T., et al. (2014). Improving mesoscale modeling using satellite-derived land surface parameters in the Pearl River Delta region, China. *Journal of Geophysical Research: Atmospheres*, 119, 6325–6346. <https://doi.org/10.1002/2014jd021871>
- Li, X., Gong, P., Zhou, Y., Wang, J., Bai, Y., Chen, B., et al. (2020). Mapping global urban boundaries from the global artificial impervious area (GAIA) data [Dataset]. *Environmental Research Letters*, 15(9), 094044. <https://doi.org/10.1088/1748-9326/ab9be3>
- Li, X., Mitra, C., Dong, L., & Yang, Q. (2018). Understanding land use change impacts on microclimate using Weather Research and Forecasting (WRF) model. *Physics and Chemistry of the Earth, Parts A/B/C*, 103, 115–126. <https://doi.org/10.1016/j.pce.2017.01.017>
- Liu, R., Han, Z., Wu, J., Hu, Y., & Li, J. (2017). The impacts of urban surface characteristics on radiation balance and meteorological variables in the boundary layer around Beijing in summertime. *Atmospheric Research*, 197, 167–176. <https://doi.org/10.1016/j.atmosres.2017.07.006>
- Liu, Y., Chen, F., Warner, T., & Basara, J. (2006). Verification of a mesoscale data-assimilation and forecasting system for the Oklahoma City area during the joint urban 2003 Field Project. *Journal of Applied Meteorology and Climatology*, 45(7), 912–929. <https://doi.org/10.1175/JAM2383.1>
- Martilli, A., Clappier, A., & Rotach, M. W. (2002). An urban surface exchange parameterisation for mesoscale models. *Boundary-Layer Meteorology*, 104(2), 261–304. <https://doi.org/10.1023/A:1016099921195>
- Masson, V. (2000). A physically-based scheme for the urban energy budget in atmospheric models. *Boundary-Layer Meteorology*, 94(3), 357–397. <https://doi.org/10.1023/A:1002463829265>
- Miao, S., Chen, F., Li, Q., & Fan, S. (2011). Impacts of urban processes and urbanization on summer precipitation: A case study of heavy rainfall in Beijing on 1 August 2006. *Journal of Applied Meteorology and Climatology*, 50(4), 806–825. <https://doi.org/10.1175/2010JAMC2513.1>
- Miao, S., Li, P., & Wang, X. (2009). Building morphological characteristics and their effect on the wind in Beijing. *Advances in Atmospheric Sciences*, 26(6), 1115–1124. <https://doi.org/10.1007/s00376-009-7223-7>
- Mohan, M., & Kandya, A. (2015). Impact of urbanization and land-use/land-cover change on diurnal temperature range: A case study of tropical urban airshed of India using remote sensing data. *Science of the Total Environment*, 506, 453–465. <https://doi.org/10.1016/j.scitotenv.2014.11.006>
- Nations, U., Economic, D. O., Affairs, S., & Division, P. (2019). *World urbanization prospects: The 2018 revision*. United Nations New York. Retrieved from <https://population.un.org/wup/publications/Files/WUP2018-Report.pdf>
- Oke, T. R. (1982). The energetic basis of the urban heat island. *Quarterly Journal of the Royal Meteorological Society*, 108(455), 1–24. <https://doi.org/10.1002/qj.49710845502>
- Oke, T. R. (1987). *Boundary layer climates*. Routledge Co.
- Oke, T. R., & Stewart, I. D. (2012). Local climate zones for urban temperature studies. *Bulletin of the American Meteorological Society*, 93(12), 1879–1900. <https://doi.org/10.1175/bams-d-11-00019.1>
- Ren, C., Cai, M., Li, X., Zhang, L., Wang, R., Xu, Y., & Ng, E. (2019). Assessment of local climate zone classification maps of cities in China and feasible refinements. *Scientific Reports*, 9(1), 1–11. <https://doi.org/10.1038/s41598-019-55444-9>
- Salamanca, F., Krpo, A., Martilli, A., & Clappier, A. (2010). A new building energy model coupled with an urban canopy parameterization for urban climate simulations—Part I: Formulation, verification, and sensitivity analysis of the model. *Theoretical and Applied Climatology*, 99(3), 331–344. <https://doi.org/10.1007/s00704-009-0142-9>
- Salamanca, F., Martilli, A., Tewari, M., & Chen, F. (2011). A study of the urban boundary layer using different urban parameterizations and high-resolution urban canopy parameters with WRF. *Journal of Applied Meteorology and Climatology*, 50(5), 1107–1128. <https://doi.org/10.1175/2010JAMC2538.1>
- Salamanca, F., Martilli, A., & Yagüe, C. (2012). A numerical study of the Urban Heat Island over Madrid during the DESIREX (2008) campaign with WRF and an evaluation of simple mitigation strategies. *International Journal of Climatology*, 32(15), 2372–2386. <https://doi.org/10.1002/joc.3398>
- Salamanca, F., Zhang, Y., Barlage, M., Chen, F., Mahalo V., A., & Miao, S. (2018). Evaluation of the WRF-Urban modeling system coupled to Noah and Noah-MP land surface models over a semiarid urban environment. *Journal of Geophysical Research: Atmospheres*, 123, 2387–2408. <https://doi.org/10.1002/2018JD028377>
- Salamanca, F. P., & Mahalov, A. (2019). Summer-and wintertime variations of the surface and near-surface urban heat island in a semiarid environment. *Weather and Forecasting*, 34(6), 1849–1865. <https://doi.org/10.1175/WAF-D-19-0054.1>
- Schatz, J., & Kucharik, C. J. (2015). Urban climate effects on extreme temperatures in Madison, Wisconsin, USA. *Environmental Research Letters*, 10(9), 094024. <https://doi.org/10.1088/1748-9326/10/9/094024>
- Shen, C., Chen, X., Dai, W., Li, X., Li, W., Fan, Q., et al. (2019). Impacts of high-resolution urban canopy parameters within the WRF model on dynamical and thermal fields over Guangzhou, China. *Journal of Applied Meteorology and Climatology*, 58(5), 1155–1176. <https://doi.org/10.1175/JAMC-D-18-0114.1>
- Shen, C., Shen, A., Cui, Y., Chen, X., Liu, Y., Fan, Q., et al. (2022). Spatializing the roughness length of heterogeneous urban underlying surfaces to improve the WRF simulation-part 1: A review of morphological methods and model evaluation. *Atmospheric Environment*, 270, 118874. <https://doi.org/10.1016/j.atmosenv.2021.118874>
- Souma, K., Tanaka, K., Suetsugi, T., Sunada, K., Tsuboki, K., Shinoda, T., et al. (2013). A comparison between the effects of artificial land cover and anthropogenic heat on a localized heavy rain event in 2008 in Zoshigaya, Tokyo, Japan. *Journal of Geophysical Research: Atmospheres*, 118, 11600–11611. <https://doi.org/10.1002/jgrd.50850>
- Stensrud, D. J. (2009). *Parameterization schemes: Keys to understanding numerical weather prediction models*. Cambridge University Press.
- Stewart, I. D., & Oke, T. R. (2012). Local climate zones for urban temperature studies. *Bulletin of the American Meteorological Society*, 93(12), 1879–1900. <https://doi.org/10.1175/BAMS-D-11-00019.1>
- Streutker, D. R. (2010). A remote sensing study of the urban heat island of Houston, Texas. *International Journal of Remote Sensing*, 23(13), 2595–2608. <https://doi.org/10.1080/01431160110115023>

- Sun, Y., Zhang, N., Miao, S., Kong, F., Zhang, Y., & Li, N. (2021). Urban morphological parameters of the main cities in China and their application in the WRF model. *Journal of Advances in Modeling Earth Systems*, 13. <https://doi.org/10.1029/2020MS002382>
- Vahmani, P., Sun, F., Hall, A., & Ban-Weiss, G. (2016). Investigating the climate impacts of urbanization and the potential for cool roofs to counter future climate change in Southern California. *Environmental Research Letters*, 11(12), 124027. <https://doi.org/10.1088/1748-9326/11/12/124027>
- Wang, S., Hu, D., Yu, C., Chen, S., & Di, Y. (2020). Mapping China's time-series anthropogenic heat flux with inventory method and multi-source remotely sensed data. *Science of the Total Environment*, 734, 139457. <https://doi.org/10.1016/j.scitotenv.2020.139457>
- Wang, X., Miao, S., Liu, H., Sun, J., Zhang, N., & Zou, J. (2019). Assessing the impact of urban hydrological processes on the summer-time urban climate in Nanjing using the WRF Model. *Journal of Geophysical Research: Atmospheres*, 124, 12683–12707. <https://doi.org/10.1029/2019JD030674>
- Yang, B., Yang, X., Leung, L. R., Zhong, S., Qian, Y., Zhao, C., et al. (2019). Modeling the impacts of urbanization on summer thermal comfort: The role of urban land use and anthropogenic heat. *Journal of Geophysical Research: Atmospheres*, 124, 6681–6697. <https://doi.org/10.1029/2018JD029829>
- Yang, L., Li, Q., Yuan, H., Niu, Z., & Wang, L. (2021). Impacts of urban canopy on two convective storms with contrasting synoptic conditions over Nanjing, China. *Journal of Geophysical Research: Atmospheres*, 126, e2020JD034509. <https://doi.org/10.1029/2020JD034509>
- Zhang, G., Zeng, G., Liang, X. Z., & Huang, C. (2021). Increasing heat risk in China's urban agglomerations. *Environmental Research Letters*, 16(6), 064073. <https://doi.org/10.1088/1748-9326/ac046e>